GEOFORSCHUNGSZENTRUM POTSDAM
STIFTUNG DES ÖFFENTLICHEN RECHTS

Scientific Technical Report

A reanalysis and reinterpretation of geodetic and geological evidence of glacial-isostatic adjustment in the Churchill region, Hudson Bay

Detlef Wolf, Volker Klemann, Johann Wünsch, Fei-Peng Zhang

Abstract

We review the historical, geological, tide-gauge, GPS and gravimetric evidence advanced in favour of or against continuing land uplift around Hudson Bay, Canada. After this, we reanalyse the tide-gauge and GPS data for Churchill using longer time series than those available to previous investigators. The dependence of the mean rate of relative sea-level change obtained on the length and mid-epoch of the observation interval considered is investigated by means of the newly developed linear-trend analysis diagram. For studying the shorter-period variability of the tide-gauge record, the continuous-wavelet transform is used. The mean rate of land uplift obtained from GPS is based on a new analysis using IGS solutions of GFZ. Furthermore, sea-level indicators from the Churchill region representing the relative sea-level history during the past 8000 a are included. Finally, the four types of observable are jointly inverted in terms of mantle viscosity. The optimum values are $\sim 3 \times 10^{20}$ Pa s and 1.6×10^{22} Pa s for the upper- and lower-mantle viscosities, respectively.

Key words: Absolute gravimetry, glacial-isostatic adjustment, GPS, linear-trend analysis, mantle viscosity, sea-level indicator, tide gauge, wavelet-transform analysis.

Contents

List of Figures

List of Tables

1   Introduction

The present-day as well as post- and late-glacial changes of the level of the sea or the height of the land can be measured using a variety of observational techniques. Apart from geological methods based on geomorphologic or organic indicators of the former sea level, several geodetic methods have been introduced to measure the present-day changes. Most prominent among them are tide-gauge measurements, which record the relative motion between land and sea, GPS measurements, which determine the topographic-height changes of the land, and absolute-gravimetry measurements, which provide an indirect measure of the disequilibrium causing these changes.

In the formerly glaciated regions of the northern hemisphere, several fundamental geodetic stations have been established, which allow us to record the ongoing adjustment of the viscoelastic earth to the last deglaciation using several types of measurement. Among them is Metsähovi, Finland, where GPS, VLBI and absolute gravimetry – supplemented by the nearby tide gauge at Helsinki – can be used to record the readjustment. The same combination of observational techniques exists at Ny-Ålesund, Svalbard, and was used to study effects due to the last deglaciation and recent ice-mass changes (Hagedoorn & Wolf, 2003). In North America, tide-gauge, GPS and absolute-gravimetry measurements are available for Churchill, Canada, and were discussed in terms of glacial isostasy (Tushingham, 1992).

In the following, we will first review the historical and geological evidence advanced in favour of or against present-day land uplift in the Hudson Bay region (Sec. 2). After this, we discuss previous analyses of the Churchill tide-gauge record and present a new analysis of it using a time series from 1940–2001 (Sec. 3). This is followed by a review of previous analyses of absolute-gravimetry and GPS measurements at Churchill and a new GPS analysis based on a time series from 1996–2003 (Sec. 4). Then, we give an overview of previous studies of the history of late- and post-glacial sea level in the Hudson Bay region and compile the indicators of former sea level from the Churchill region used in this study (Sec. 5). Finally, we review estimates of the mantle viscosity based on the late- and post-glacial sea-level history around Hudson Bay proposed by other investigators and present a new estimate based on a joint inversion of the complete geological and geodetic data base available for the Churchill region (Sec. 6). Our study concludes with a brief summary of the main results achieved (Sec. 7).

2 Historical and geological evidence of present-day land uplift

The first suggestion that the land around Hudson Bay continues to rise is probably due to Bell. In several official reports of the Geological Survey of Canada published between 1875 and 1886, he described the various evidence supporting his hypothesis. Most of his 'proofs' were later compiled in Bell (1896). In this publication, he noted there that, since the establishment of the posts of the Hudson's Bay Company around 1700 in the mouths of several rivers entering into the bay, it had become increasingly difficult to reach the posts from the sea. An example is Little Whale River near Richmond Gulf, which had to be abandoned as a harbour. Of interest to Bell was in particular the situation in Sloops Cove near Churchill, where larger ships wintered during the 18th century and which had become difficult to reach even for row boats when Bell visited the cove. Important evidence to him was also partially rotten driftwood, which he had noticed along the east coast at heights of 15–25 m above the reach of the highest tides. The wood was arranged along even lines, with the material freshest at the lower altitudes and becoming progressively more decayed with increasing elevation. Bell found similar evidence in gravel terraces, which were sharp and fresh-looking, or in indications of the drying out of marshes or the advance of growth. Bell also quoted aboriginal geographical names or historical notes suggesting a recent uplift of the land, the appearance of new islands or changes from islands to peninsulae. Meaningful to him were also beach dwellings and fish traps built from rock by the Innuit, which were found at all elevations up to ~20 m. Summarizing the evidence, he concluded that the question of the continuation of the post-glacial land uplift around Hudson Bay could be answered in an affirmative way and suggested an uplift rate of 1.5–3 m per century and, in particular, of ~2.1 m per century for the Churchill region.

Bell's views were challenged by Tyrrell (1896), who noted that the location of Fort Prince of Wales at Churchill during his visit was such that it could not have been high enough above the storm waves when constructed in 1733, if the land uplift had been ~3.3 m since that time (which corresponds to ~2.1 m per century). He also reproduced a map published in 1752 according to a survey up the Churchill River around 1746, which showed high- and low-water limits and marshy grounds as they existed more than a hundred years later. Furthermore, he reported that, on November 2, 1893, he had measured the heights of six names associated with calendar years (1741–1757, those of 1753 were also dated May 27) engraved in the rocky walls of Sloops Cove. Considering that, during winter, the cove becomes regularly filled with ice up to the level of the highest spring tide of that winter, Tyrrell concluded that the dated names (2.1 m above the level of the ice on November 2, 1893) had doubtlessly been cut while the ice in the cove had been at the peak level of the winter of 1753

(the mean break-up date is June 19). Since the ice on November 2, 1893 had been at the level of the ordinary spring tide of October 27, 1893 (Tyrrell, 1894) and, thus, ∼0.3 m lower than on May 27, 1753, this peak level would be ∼1.8 m below the names and, with a snow cover on May 27, 1753, the value could even be lower. To Tyrrell, this indicated that the water had been about as high with respect to the names when the names were cut as it had been in 1893. This conclusion was in contrast to Bell (1896), who noted that the men might have been sitting rather than standing while cutting their names. As a further indication against continuing land uplift, Tyrrell also pointed out that the 'Furnace' – a small ship that had spent the winter of 1741/1742 in Sloops Cove – had a draft of no more than 1.8 m when lightened, but could pass the entrance to the cove only at high tide. However, at Tyrrell's time, the depth of the entrance was still ∼1.2 m and, furthermore, any decrease in depth of the bottom of the cove from 1.8 m to 1.2 m might also have been due to the accumulation of silt as a consequence of an artificial dam built from rock fragments at the mouth of the cove for protection. Tyrrell also noted that rings for mooring ships existed in Sloops Cove near 1.5 m above the ice, which – although they had been doubtlessly placed there in the middle of the 18th century – were still firm and strong. Taken together, the evidence indicated to him that no significant land uplift had occurred near Churchill over a century and a half.

Johnston (1939) revisited the 'Sloops Cove problem' and reported that the heights of the six names in the cove used by Tyrrell (1894, 1896) had been levelled with reference to the low-water datum of the CHS charts by the Department of Railways and Canals (later Department of Transport) on September 26, 1934. He published a table with the heights of the names in feet. After converting Tyrrell's heights to the new reference, the differences were within the uncertainties of the method. To Johnston, this confirmed Tyrrell's conclusion as to the absence of any definite indications of recent land uplift. This is in contrast to results of a field survey carried out by Stanley (1939), who confirmed Bell's (1896) evidence of unrotten driftwood ∼25 m above sea level, although he admitted the slowness of decay in the cold climate.

Tyrrell's (1894, 1896) conclusion of no clear indications of recent land uplift around Churchill was also supported by Moore (1948), who extrapolated the line of zero vertical movement in the Great Lakes region towards north on the assumption of a roughly circular shape of this line and concluded that it should pass somewhere near Churchill. Interestingly, the results indicating present-day stability of the land around Hudson Bay were later picked up by Jeffreys (1952, 1976) as an argument against the possibility of viscous flow in the earth's interior.

In his first analysis of the tide-gauge data for Churchill, Gutenberg (1941) also revisited the 'Sloops Cove problem' and pointed out that Tyrrell's (1894, 1896) and Johnston's (1939) reasoning had been based on the assumption that, on May 27, 1753, the ice surface was still 4.5–4.8 m above the height of the

contemporary sea level. However, if the ice had broken up before – which had happened not infrequently in more recent years –, a land uplift of more than 3 m in 180 years would be indicated. Cooke (1942) briefly reviewed Tyrrell's qualitative evidence and concluded that Gutenberg's inference of land uplift around Churchill had been premature. In his rebuttal, Gutenberg (1942) emphasized that the indications given by Tyrrell were interpreted by him merely as excluding subsidence of the land.

Later, Manning (1951) reinvestigated the driftwood strandlines in James Bay and, in particular, studied the possibility that they might have been formed by extraordinary storm tides. His conclusion was that the appearance of the highest driftwood strandlines could only be accounted for by land uplift since their formation. Manning, therefore, essentially confirmed the explanation of the driftwood strandlines first proposed by Bell (1896), who, however, had not considered the problem of storm tides in detail.

The question of present-day land uplift around Hudson Bay was once more reviewed by Bird (1954). In addition to the evidence advanced by the earlier investigators, he quoted inhabitants of Baker Lake, who had noticed that the lake had retreated since the establishment of the settlement in the 1920s. Also, older Innuit agreed that, between Chesterfield Inlet and Eskimo Point, rocks had appeared since their youth. Bird furthermore referred to archaeological sites that indicated a land uplift of ∼24 m since the arrival of the Dorset culture and of ∼9 m since the arrival of the Thule culture (no absolute ages were available to Bird).

Convincing geological evidence of continuing land uplift had to await the advent of the ^{14}C dating method in the 1950s. Of particular interest are the studies by Fairbridge & Hillaire-Marcel (1977) and Hillaire-Marcel & Fairbridge (1978). Using a staircase of 185 beach ridges found along the east coast of Hudson Bay, they constructed a continuous record of emergence from ∼8300 a BP (sidereal) to present time. Their result was based on a newly discovered (45 ± 5) a cycle in beach building believed to correspond to periods of storminess and high tides. Of particular interest is that the altitudinal spacing of the shorelines becomes progressively closer as they approach the modern shoreline, indicating that land uplift has been gradually decreasing with time. In the Richmond Gulf region, a contemporary uplift of ∼11 mm/a is indicated on the basis of this evidence.

3 Tide-gauge evidence of present-day land uplift

To monitor the long-term RSL trends on regional to global scales, tide gauges continue to be a useful technique (*e.g.* Lisitzin, 1974; Emery & Aubrey, 1991; Douglas et al., 2001). For sets of globally distributed stations, the long-term trends have recently been determined and discussed by, for example, Douglas (1991, 1997), who favours time series of at least 70 a to eliminate interannual and decadal variations. At present, estimates of the globally averaged rate of RSL-height change range between 1 and 2 mm/a, with a central value of 1.5 mm/a (*e.g.* Meier & Wahr, 2002). Whereas part of this rise is probably related to the recent melting of mountain glaciers and ice caps, the major portion appears to be caused by the thermal expansion of sea water (*e.g.* Peltier & Douglas, 2002).

An interfering contribution arises from the earth's GIA following the retreat of the last Pleistocene ice sheets. This effect is particularly obvious in the once ice-covered regions of Fennoscandia and Canada, where pronounced RSL fall caused by deglacial land uplift results. In Fennoscandia, the contemporary land uplift has been monitored by more than 40 tide-gauge stations with a record length of at least 50 a (*e.g.* Plag, 1988; Ekman, 1996; Lambeck et al., 1998). In Canada, most of the long-term tide-gauge stations are located along the east coast (Vaníček & Nagy, 1979) and, thus, away from the uplift centre. Close to the uplift centre, Churchill is the location of the only tide-gauge station with an observation record exceeding 50 a, which will be reviewed in the following.

3.1 Previous analyses

A quantitative method of deciding the question whether the land around Hudson Bay is still rising was provided when a tide-gauge was deployed at Churchill in September 1928. The first attempt to use this type of evidence was due to Gutenberg (1941). Since the early operations were interrupted during winter due to ice, records were initially available only for the summer months. To eliminate the annual period due to melting of the ice and flow of the Churchill River, Gutenberg calculated the mean rate of RSL-height change separately for each month of the observation interval 1928–1939. His results were −39 mm/a (June), −26 mm/a (July), −22 mm/a (August), −12 mm/a (September), −30 mm/a (October) and −45 mm/a (November), which gives a mean of −29 mm/a (not calculated by Gutenberg, who favoured a rate near −20 mm/a).

Gutenberg's (1941) results were rejected by Cooke (1942), who pointed out several problems associated with the Churchill tide-gauge record. In particular, he objected that the tide gauge was not located on the open coast of Hudson Bay, which causes its record to be influenced by the inflow of the

Table 1: Previous estimates of observational mean rate of RSL change, $\bar{\dot{s}}_{\mathrm{obs}}$, their standard error, ϵ, and standard deviation, σ, based on monthly RSL heights for Churchill and linear regression. The original data were provided by CHS (Gutenberg, 1941, 1942, 1954), MEDS and MSB (Barnett, 1966, 1970). The rate of Gutenberg (1941) is the mean of his separate rates for the months June–November, the rates of Gutenberg (1942) apply to the months June–November (first line) and August–October (second line), the rate of Gutenberg (1954) is based on the months July–September, the other rates were calculated from all monthly RSL heights available. The rate of Barnett (1966) was corrected by Barnett (1970).

Author(s)	Obs. interval	$\bar{\dot{s}}_{\mathrm{obs}}$ (mm/a)	ϵ (mm/a)	σ (mm)
Gutenberg (1941)	1928–1939	−29.0	–	–
Gutenberg (1942)	1928–1940	−25.0	7.5	–
	1928–1940	−22.5	7.5	–
Gutenberg (1954)	1929–1951	−10.5	1.8	–
Barnett (1966)	1940–1964	−4.1	–	–
Dohler & Ku (1970)	1940–1967	−3.9	0.7	–
Barnett (1970)	1940–1968	−3.9	–	–
Vaníček & Nagy (1979)	1940–1975	−4.5	0.3	–
Tushingham (1992)	1940–1991	−8.8	0.3	113
Tushingham (1992)	1940–1975	−4.4	0.5	94
Tushingham (1992)	1977–1991	−8.8	2.4	123

Churchill River and the narrow mouth of the harbour. Cooke therefore suggested to restrict the analysis to the months of August–October, when the river flow is low and, therefore, the differences to the open sea are likely to be small. He furthermore noted that the tide-gauge readings showed no regular change. Instead, since 1928, they had stayed essentially constant until late August or early September 1934. At this time, they showed a drop of nearly 30 cm and again stayed essentially constant afterwards. Cooke emphasized that this is not the behaviour typical of regularly rising land. However, if the land uplift did occur in a series of jerks, then, in order to calculate a mean rate, it would be necessary to know more about the statistics of the ground motion than could be extracted from the short Churchill record.

In his response, Gutenberg (1942) pointed out that he had used the method of linear regression of the monthly RSL heights, separately for each month, to estimate the mean rate of RSL-height change. He also noted that local effects, such as river flow and harbour conditions, were unlikely to affect trends over 13 years. Based on linear regression, Gutenberg then calculated new rates of

RSL-height change for the slightly extended observation interval 1928–1940, which were (-25.0 ± 7.5) mm/a (June–November) and (-22.5 ± 7.5) mm/a (August–October).

Since the validity of the Churchill tide-gauge record and its interpretation by Gutenberg continued to be questioned (Moore, 1948; Bird, 1954), the problem was revisited by him (Gutenberg, 1954). After once more reviewing the early studies by Tyrrell (1894, 1896) and Johnston (1939), Gutenberg first noted that one reason for continuing objections to the hypothesis of contemporary land uplift around Hudson Bay appeared to be that observations on the North American continent were much more sparse and had been misinterpreted much more frequently than for Fennoscandia. Gutenberg then concluded that the studies by Tyrrell, Johnston and others suggesting stability were consistent with a moderate land uplift, but that the errors involved were too large for a reliable numerical value. In view of the inconclusive historical and geological evidence, Gutenberg advanced a new interpretation of the Churchill tide-gauge record. Limiting his analysis to the 'quiet' months July–September, linear regression of the monthly RSL heights for the observation interval 1929–1951 returned (-10.5 ± 1.8) mm/a as the mean rate of RSL-height change.

Later, Gutenberg (1958) discussed the Churchill tide-gauge data for the last time and considered the irregularity of the record as typical of such records and probably related to 'meteorological' influences. He also pointed out that a temporary blocking of the subcrustal flow causing the land uplift might be responsible for this irregularity. Nevertheless, the accuracy of the Churchill tide-gauge readings continued to be questioned and the rates calculated by Gutenberg regarded as unreliable (Bird, 1959; Farrand & Gajda, 1962).

A fresh attempt to analyse the Churchill tide-gauge data was undertaken by Barnett (1966). As he pointed out, the data from Churchill were probably among the least reliable, but among the most significant in support of Gutenberg's (1941) conclusion of continuing land uplift in North America. In a brief review of the technical aspects, Barnett noted that, until 1940, the tide gauge had been operated in the summer months for the Department of Mines and Technical Surveys by different agencies. During that time, the annual removal and reinstallation of the instrument were potential sources of error. Also, the original records did not show indications of regular level controls each time the gauge had been moved. After 1940, the operation was transferred to MSB belonging to the same department, and an automatic tide gauge was put into operation. At the same time, the records were referred to the permanent bench mark 566-D at Cape Merry, and the topographic height of the instrument was checked annually by levelling. Furthermore, a continuous record became possible by maintaining the tide gauge in a heated well connected with the sea in the winter and operating it in the harbour wharf in the summer. In 1956, the instrument was relocated and remained at the same position all year round. In 1963, it was moved to a special gauge house.

In view of the operational problems before 1940, Barnett (1966) restricted his analysis of the Churchill tide-gauge data to the observation interval 1940–1964 and, based on linear regression of the full set of monthly RSL heights, calculated a mean rate of RSL-height change of -6.1 mm/a. A later check revealed that the rate was in fact -4.1 mm/a for this interval and -3.9 mm/a for the extended interval 1940–1968 (Barnett, 1970). This value agrees with that obtained by Dohler & Ku (1970), whose linear-regression analysis for the observation interval 1940–1967 returned (-3.9 ± 0.7) mm/a. Obviously, the new rates are significantly less than those determined by Gutenberg (1941, 1942, 1954).

Walcott (1972) discussed Barnett's (1970) estimate of the mean rate of RSL-height change at Churchill and noted that it was smaller in magnitude than the relative rates inferred from tide gauges for the Lake Superior basin. Walcott therefore concluded that the Churchill value must be treated with caution. If correct, however, it would indicate that the region of largest uplift has migrated southeast during the last several thousand years. When compiling a map of recent crustal movement for Canada, Vaníček & Nagy (1979) later analysed the extended observation interval 1940–1975 using monthly RSL heights provided by MEDS. Also based on linear regression, they calculated a mean rate of RSL-height change of (-4.5 ± 0.4) mm/a for Churchill and, thus, essentially confirmed Barnett's (1970) results.

The first indication of a larger present-day land uplift, in fact, results from the relevelling of bench mark 566-D at Cape Merry by the GSD in 1978. As Hansell et al. (1983) reported, a land-uplift rate of 8.15 mm/a was obtained from this survey.

More than a decade later, Tushingham (1992) presented another reanalysis of the Churchill tide-gauge record. Employing monthly RSL heights from MEDS and linear regression, he obtained a mean rate of RSL-height change of (-8.3 ± 0.8) mm/a for the extended observation interval 1940–1991. Since the Churchill record is expected to be influenced by annual changes, he also computed rates based on the monthly RSL heights for particular months, which ranged from ~-7 mm/a (February) to ~-10 mm/a (December). A possibly significant complication mentioned by Tushingham concerns the Churchill River Diversion Project between 1975 and 1977, which resulted in the flooding of vast regions $\sim$300 km upriver and a 60% diversion of the runoff of Churchill River into Nelson River further south. Since a positive correlation was found between the rate of discharge for Churchill River and the RSL height at Churchill harbour, the drastic reduction in outflow around 1976 may have had a significant effect on the tide-gauge record. To study the potential effect of the diversion, Tushingham divided the complete observation interval into pre- and post-diversion intervals and obtained rates of (-4.4 ± 0.5) mm/a (1949–1975) and (-8.8 ± 2.4) mm/a (1977–1991). As he pointed out, the pre-diversion rates compare favourably with the rates determined by Barnett (1966, 1970) and Vaníček & Nagy (1979), whereas the post-diversion rates are

probably unreliable because of the shortness of the record and its gaps. The various estimates of the observational mean rate of RSL-height change, $\bar{\dot{s}}_{\mathrm{obs}}$, their standard error, ϵ, and standard deviation, σ, are listed in Table 1.

The most recent analysis is due to Gough & Robinson (2000). Studying the annual variation of the Churchill tide-gauge record more closely, they pointed out that it is characterized by a double amplitude of $\sim$300 mm before 1975 and $\sim$350 mm after 1975. Based on statistical analysis, they found that the Churchill River discharge is responsible for $\sim$43% of this variability, whereas $\sim$18% are contributed by the Nelson River discharge. The increase in the annual variation after 1975 could be linked to the Churchill River diversion after 1975. In their discussion of linear trends, Gough & Robinson divided the observation interval into 1950–1970, 1970–1985 and 1985–1998 and estimated the rate of RSL-height change as -3 to -4 mm/a, -20 mm/a and close to zero, respectively, for the three sub-intervals. In contrast to Tushingham (1992), they argued that the Churchill River diversion occurred too late to be responsible for the increased RSL fall beginning in 1970. In their search for an alternative explanation, they pointed out that, during 1960–1975, the global mean temperature dropped, whereas, after 1975, it rose. Considering continental ice-mass changes and thermal expansion of the ocean water with a lag of 10 a, they showed that the expected RSL-height change is roughly consistent with the changes in linear trend observed.

3.2 New analyses based on PSMSL time series

Whereas Tushingham (1992) considered MEDS data for 1940–1991, monthly RSL heights are now available from PSMSL for 1940–2001 via internet (http://www.pol.ac.uk/psmsl/). Figure 1 shows the PSMSL time series of monthly RSL heights for Churchill. An annual cycle nearly proportional to $-\sin\omega t$, where t is the time with respect to the beginning of a calendar year, with an amplitude of $\sim$96 mm is indicated. We also note an upward spike for the fall of 1997, which may be related to the 1997 El Niño event.

To calculate the mean rate of RSL-height change, linear regression of the monthly RSL heights is used. Following Vaníček & Nagy (1979), we approximate the time series by

$$s_{\mathrm{LR}}(t) = a + \bar{\dot{s}}_{\mathrm{obs}}t, \tag{1}$$

where s_{LR} is the RSL height based on linear regression, a the intercept, $\bar{\dot{s}}_{\mathrm{obs}}$ the observational mean rate of RSL-height change and t the time epoch. From linear regression, we have

$$a = \frac{\sum s_n - \bar{\dot{s}}_{\mathrm{obs}} \sum t_n}{N}, \tag{2}$$

$$\bar{\dot{s}}_{\mathrm{obs}} = \frac{N \sum t_n s_n - \sum t_n \sum s_n}{N \sum t_n^2 - (\sum t_n)^2}, \tag{3}$$
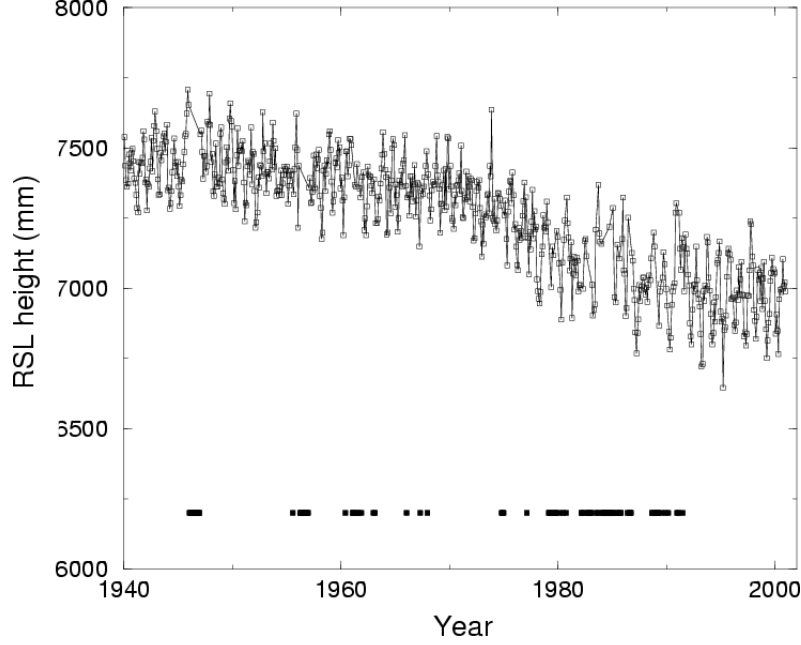
Figure 1: Monthly RSL height at Churchill according to PSMSL data. The horizontal bars indicate data gaps.

where s_n is the monthly RSL height for the nth month, t_n the reference time epoch for s_n (taken at the mid-epoch of the month) and N the total number of monthly values considered. The standard deviation, σ, of s_{obs} is given by

$$\sigma = \sqrt{\frac{\sum s_n^2 - a \sum s_n - \bar{\bar{s}}_{\mathrm{obs}} \sum t_n s_n}{N-2}} \, . \tag{4}$$

The standard error, ϵ, of $\bar{\bar{s}}$ is calculated according to

$$\epsilon = \sqrt{\frac{N\sigma^2}{N \sum t_n^2 - (\sum t_n)^2}} \, . \tag{5}$$

Linear-regression analysis for the complete observation interval ($N = 642$ monthly RSL heights for 732 months = 61 a) yields a mean rate of RSL-height change of $\bar{\bar{s}}_{\mathrm{obs}} = (-9.72 \pm 0.26)$ mm/a with a standard deviation of $\sigma = 116$ mm (Table 2). Also listed are the mean rates of RSL-height change for the sub-intervals 1940–1975 and 1975–2001. As found by Tushingham (1992), the value of $\bar{\bar{s}}_{\mathrm{obs}} = (-4.44 \pm 0.45)$ mm/a for the first sub-interval is much smaller in magnitude than that of $\bar{\bar{s}}_{\mathrm{obs}} = (-10.41 \pm 0.95)$ mm/a for the second sub-interval.

As a further control, the IB reduction (*e.g.* Lambeck, 1980) has been applied to the Churchill tide-gauge data. The air-pressure data base used for this

Table 2: Revised estimates of observational mean rate of RSL change, $\bar{\dot{s}}_{\mathrm{obs}}$, their standard error, ϵ, and standard deviation, σ, based on N monthly RSL heights for Churchill (PSMSL No. 970141, 58.78°N, 94.20°W) and linear regression. The original RSL heights were provided by PSMSL. The IB reduction implied for the last line is based on GMSLP2.1f air-pressure data provided by BADC.

Obs. interval	N	$\bar{\dot{s}}_{\mathrm{obs}}$	ϵ	σ
		(mm/a)	(mm/a)	(mm)
1940–2001	642	−9.72	0.26	116
1940–1975	394	−4.44	0.45	94
1975–2001	260	−10.41	0.95	121
1940–1994	551	−9.43	0.32	115
1940–1994 (IB)	551	−9.65	0.28	102

reduction is GMSLP2.1f (Basnett & Parker, 1997), which is a global archive of historical, monthly sea-level pressure data provided by BADC. The air-pressure data are gridded with a spatial resolution of $5° \times 5°$, the observation interval is 1871–1994. Since the geographical coordinates of the tide-gauge station at Churchill are 58.78°N, 94.20°W, the closest grid-point in GMSLP2.1f is 60°N, 95°W.

The IB reduction is based on the assumption that the air-pressure variations change the sea level hydrostatically. Numerically, the reduction adds 1 cm to the RSL height per 1 mbar pressure in excess of 1013 mbar and vice versa. Values for the mean rate of RSL-height change for the sub-interval 1940–1994 with and without IB reduction are also given in Table 2. Whereas there is only a small difference in the rates (−9.65 mm/a with IB reduction versus −9.43 mm/a without IB reduction), the standard deviation, σ, is markedly smaller if the IB reduction is applied (102 mm with IB reduction versus 115 mm without IB reduction).

3.3   New analyses based on UHSLC and MEDS time series

For the observation interval 1995.042–2000.958 (71 months, one month is missing in the UHSLC time series), three time series of monthly RSL heights have been computed and compared as a quality control of the Churchill tide-gauge data. The first series consists of the PSMSL monthly RSL heights. This data set implies a reduction to a common reference on the basis of the tide-gauge datum history as reported by the operating authority. So far, the data of approximately two thirds of the PSMSL stations have been reduced in this way and form the revised local reference (RLR) data set. The second series consists of monthly RSL heights distributed by UHSLC via internet (http://uhslc.soest.hawaii.edu/uhslc/jasl.html). These are raw data not ad-
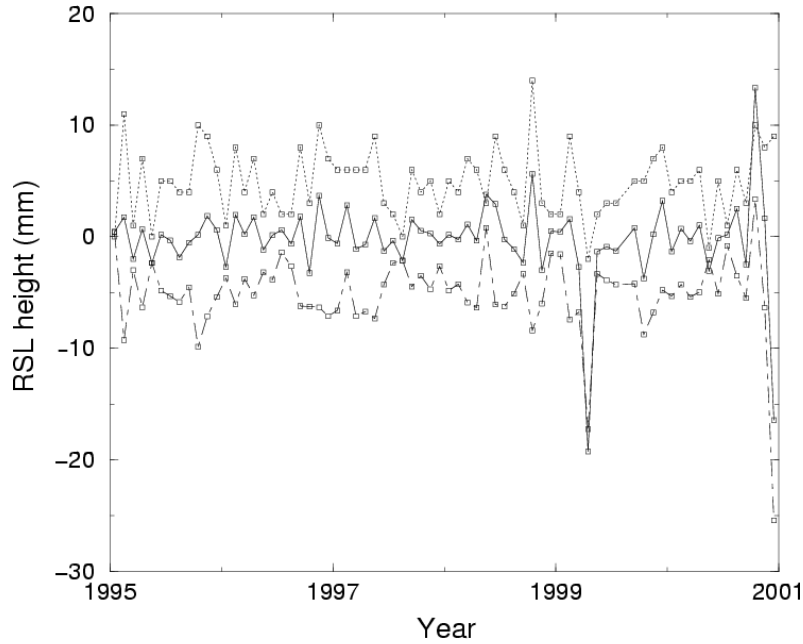
Figure 2: Differences between monthly RSL heights at Churchill. UHSLC minus filtered CHS (solid), UHSLC minus PSMSL (dotted), PSMSL minus filtered CHS (dot-dashed).

justed to the RLR system. The third series is based on hourly RSL heights provided by CHS. After applying a boxcar-filter program provided by MEDS to the data, daily RSL heights are obtained, from which monthly RSL heights can be calculated. The program implements boxcar filters with 24-h and 25-h windows, which largely suppress the semi-diurnal and diurnal lunisolar tides present in the hourly RSL heights.

Figure 2 shows the monthly differences between the three time series, *i.e.* UHSLC minus filtered CHS, UHSLC minus PSMSL and PSMSL minus filtered CHS as functions of time. The curves have been shifted by constant amounts for ease of comparison. The outliers at the end of the observation interval possibly reflect truncation effects of the filter, the reason for the outliers at 1999.292 is not clear. The standard deviations of the differences are $\sigma = 3.9$ mm (UHSLC minus filtered CHS), $\sigma = 3.1$ mm (UHSLC minus PSMSL) and $\sigma = 3.7$ mm (PSMSL minus filtered CHS). Therefore, the UHSLC and PSMSL time series show the best agreement.

3.4   Continuous-wavelet analysis

The RSL heights for Churchill provided by PSMSL are further analysed using the continuous-wavelet transform, which can be interpreted as a truncated
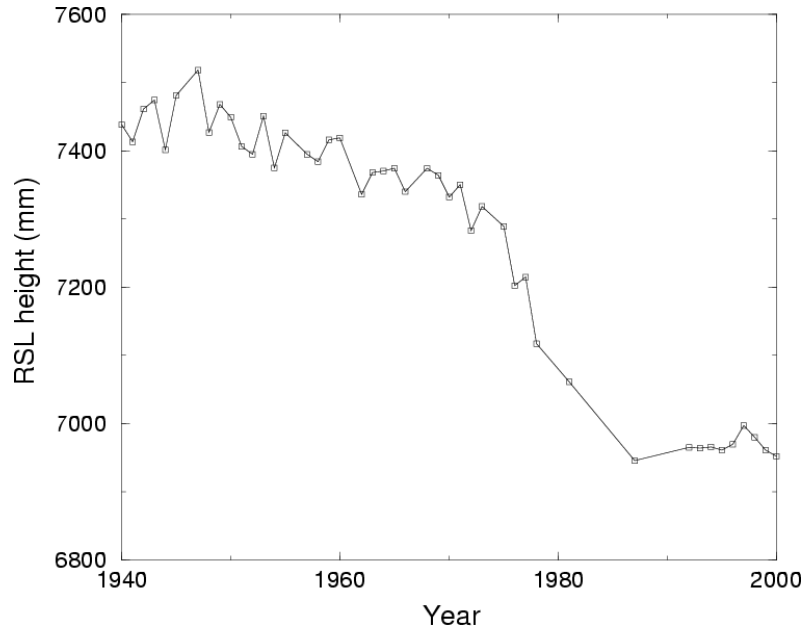
Figure 3: Annual RSL height at Churchill calculated from PSMSL data.

Fourier transform applied to a sliding time interval (*e.g.* Hubbard, 1997; Torrence & Compo, 1998).

Figure 4 displays the residual PSMSL time series of monthly RSL heights obtained after subtracting the linear trend, the analysing Morlet wavelet, the wavelet scalogram, *i.e.* the complex modulus of the amplitude, and the Fourier amplitude spectrum. Clearly shown are the annual and sub-annual periods of 1 a, 0.5 a and 0.33 a as well as a decadal period of ∼50 a. The latter is close to the period of ∼45 a noted by Fairbridge & Hillaire-Marcel (1977) when studying the late- and postglacial land uplift along the east coast of Hudson Bay. In agreement with Figure 1, the amplitude of the annual oscillation increases towards the end of the observation interval considered. Also shown is the scalogram obtained after application of the IB reduction. As expected, the amplitude of the annual period is significantly reduced in this case, whereas the other features are essentially preserved.

3.5   Linear-trend analysis

The annual RSL height at Churchill (Figure 3) shows a pronounced drop starting around 1970 and continuing for almost 15 a. After this, the annual means have remained nearly constant. To study the variability of the calculated linear trends systematically, we use a newly developed linear-trend analysis diagram (Figure 5). It shows, in a triangle, the mean rate of RSL-height change, calculated according to the method outlined in Sec. 3.2, as a function of the length of the observation interval considered and of its mid-epoch. Grey regions in-

side the triangle indicate intervals for which the hypothesis of a linear trend is refused. For a fixed interval length, the diagram displays the time dependence of the linear trend, whereas, for a fixed mid-epoch, its dependence on the interval length is shown. At the bottom corner of the triangle, the linear trend for the complete observation interval is given.

Obviously, short observation intervals are not suitable for estimating the long-term rate of RSL-height change, because the value depends strongly on the mid-epoch considered. For intermediate observation intervals of $\sim$15 a, the diagram continues to show non-uniformity, with rates of $\sim$−5 mm/a for mid-epochs of 1950–1970 and rates of $\sim$−10 mm/a for mid-epochs after 1985, which essentially confirms the results shown in Tables 1 and 2. For the observation interval in between, rates in the range of −15 to −20 mm/a apply. With increasing interval length, the different rates gradually merge. Thus, for 40 a intervals, a monotonous increase in the rate of RSL fall followed by a levelling-off towards the end of the complete observation interval results.

As discussed by Gough & Robinson (2000), the interannual and decadal RSL variations visible in Figures 4 and 5 probably represent steric effects caused by temperature or salinity variations in Hudson Bay. Since these contributions cannot be independently determined, their influence on the linear-trend estimates is unknown. We therefore regard the mean rate of RSL-height change based on the complete time series as the most reliable estimate of the GIA-induced contribution.
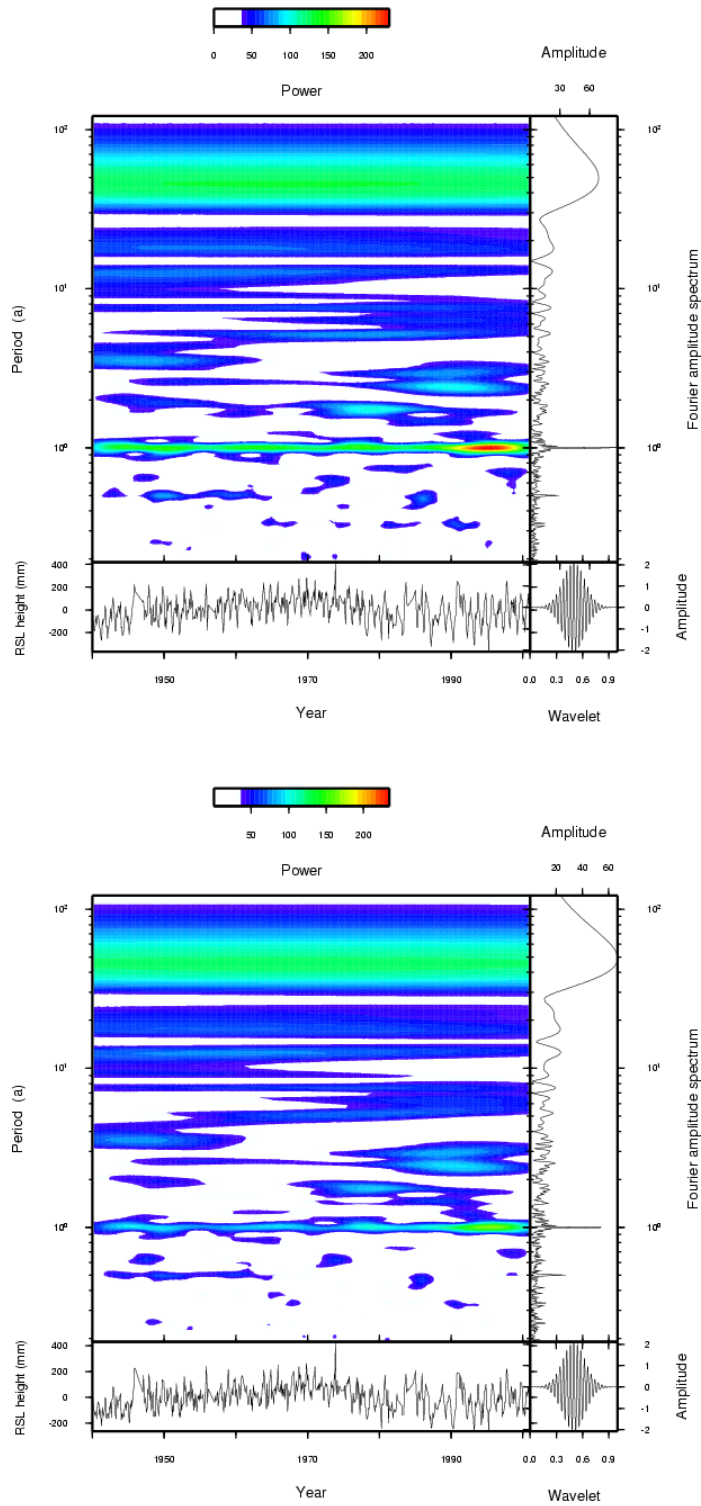
Figure 4: Continuous wavelet transform of monthly RSL height at Churchill according to PSMSL data without (top) and with (bottom) IB reduction. The panels show the wavelet scalogram (upper left), the Fourier amplitude spectrum (upper right), the detrended PSMSL time series (lower left) and the analysing Morlet wavelet (lower right).
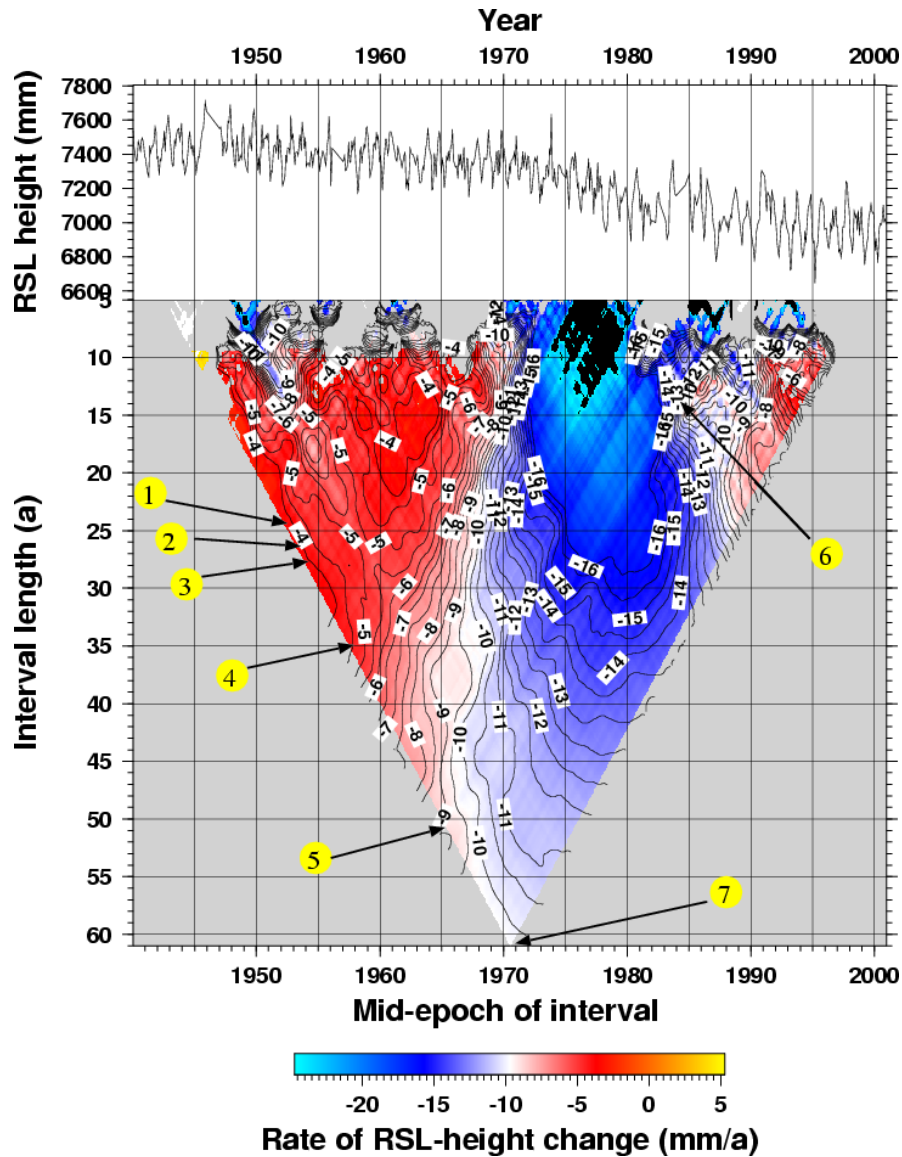
Figure 5: Linear-trend analysis diagram for monthly RSL height at Churchill according to PSMSL data. The panels show the original PSMSL time series (top) and the contour plot of the mean rate of RSL change in mm/a as a function of length and mid-epoch of the observation interval considered (bottom). Grey regions inside the triangle indicate that the hypothesis of a linear trend is refused. Arrows point to previous estimates according to (1) Barnett (1966) for 1940–1964, (2) Dohler & Ku (1970) for 1940–1967, (3) Barnett (1970) for 1940–1968, (4) Vaníček & Nagy (1979) for 1940–1975, (5) Tushingham (1992) for 1940–1991, (6) Tushingham (1992) for 1977–1991 and (7) this study for 1940–2001.

4 Absolute-gravimetry and GPS evidence of present-day land uplift

An indirect method of monitoring GIA became available with the advent of absolute gravimetry. In Canada, an absolute-gravimetry program was initiated during the late 1980s (Lambert et al., 1989) and, recently, mean rates of gravity change were estimated for the stations Churchill, Flin Flon, Pinawa, International Falls, Wausau and Iowa City located on a north–south traverse in mid-continental North America (Lambert et al., 2001). For most stations, the time series are only ∼5 a long with, typically, one measurement per year. An exception is Churchill, where measurements have been taken for more than a decade and also more frequently.

Compared to Fennoscandia, where a rather dense network of GPS stations in operation since ∼10 a has returned accurate rates of change of the displacement field (Scherneck et al., 2002), the situation is less favourable in Canada. Over the last several years, IGS stations have been in operation at Algonquin Park, Churchill, Flin Flon, Ottawa, Schefferville, St. John's, Whitehorse and Yellowknife. After 2000, they were supplemented by new stations at Baie Comeau, Baker Lake, Halifax, Kuujuarapik, Pickle Lake and Val d'Or jointly operated by GFZ and GSD.

In the following, only Churchill will be considered, where absolute-gravimetry and GPS observations started in 1987 and 1993, respectively.

4.1 Previous analyses

In an attempt to provide independent evidence of present-day isostatic adjustment, Lambert et al. (1994) proposed a first analysis of temporal gravity variations based on absolute gravimetry at Churchill conducted during nine campaigns between 1987 and 1991. Upon elimination of one anomalous value, linear regression returned a rate of gravity change of -1.6 μGal/a with a standard deviation of 2.0 μGal. Later, as more absolute-gravimetry data had become available, Lambert et al. (1996) presented a new value. Disregarding two anomalous measurements in 1990, they estimated a rate of gravity change of (-1.45 ± 0.19) μGal/a and a standard deviation of 1.6 μGal for the observation interval 1987–1995. Lambert et al. (1998) tried to improve the constraints on GIA in Manitoba by combining three types of observation: the late-glacial tilting of the Campbell shoreline of pro-glacial Lake Agassiz, the present-day tilting of southern Manitoba lakes and the present-day rate of gravity change at Churchill for the observation interval 1987–1995. Eliminating another gravity measurement regarded as anomalous and using weighted linear regression (which allows for a constant bias for each gravimeter used), they obtained an improved rate of gravity change of (-1.63 ± 0.17) μGal/a. Using the conversion factor -6.7 mm/μGal obtained from theoretical predictions, this corresponds to a rate of topographic-height change of (10.9 ± 1.1) mm/a. Lambert et al.

(1998) also compared this value with Tushingham's (1992) linear-trend estimates of the mean rate of RSL-height change for Churchill, where one of his values was $\sim(-8.5 \pm 1.0)$ mm/a. If corrected for a rate of a globally averaged rate of RSL-height change of 1.5 mm/a and a rate of geoid change of 0.9 mm/a, this returns a rate of topographic-height change of (10.9 ± 1.0) mm/a. Recently, Lambert et al. (2001) have analysed 71 gravity measurements made at six sites along a profile from Hudson Bay to Iowa during the observation interval 1987–1999. Weighted linear regression gave a rate of gravity change of (-2.13 ± 0.23) μGal/a for Churchill. This is significantly higher than predicted using ice model ICE-3G and a 'standard' earth model (Tushingham & Peltier, 1991). Lambert et al. (2001) noted that the discrepancy can be avoided either by an increase of the lower-mantle viscosity by a factor of 2–3 or by a 50% increase in thickness of ICE-3G west of Lake Superior.

Larson & van Dam (2000) analysed data from four locations in Canada and the northern USA based on at least three years of continuous GPS observations and at least two absolute-gravimetry campaigns. Although gravity changes may reflect mass changes not recorded by GPS, the mean rates determined by the two techniques agree to within one standard error at all sites (using the conversion factor -6.5 mm/μGal). The mean rates of topographic-height and gravity change determined for Churchill are, respectively, (10.7 ± 0.23) mm/a and (-1.54 ± 0.48) μGal/a (estimated from their Figure 4). Park et al. (2002) analysed GPS data for 20 selected IGS stations in north-eastern USA and midwestern Canada and determined mean rates of topographic-height change by linear regression. Compared to 'best-fitting' theoretical predictions, the value of (13.0 ± 0.33) mm/a estimated for Churchill was consistently too high by $\sim$3 mm/a.

The various estimates of the observational mean rates of topographic-height change, $\bar{u}_{\mathrm{obs}}$, and gravity change, $\bar{g}_{\mathrm{obs}}$, their standard error, ϵ, and standard deviation, σ, are listed in Table 3.

4.2   New GPS analysis based on IGS solutions

The GPS station Churchill (CHUR, 58.75°N, 94.08°W) has been operated by GSD with a continuous observation history since April 24, 1993. CHUR is one of the 273 globally distributed GPS stations selected by GFZ for the SEAL and TIGA projects. The data are processed on a daily basis using the software package EPOS (Gendt et al., 1994) developed by GFZ. For the present study, the output of EPOS are loosely constrained daily network solutions. Back to 1996, the data have been analysed in three routines. The first routine processes the data with a one-week delay. Part of the results of this routine are also used as IGS solutions by GFZ. The second routine processes the data with a 460-day delay to include late data. The third routine processes the data backwards every four weeks to obtain a quick overview of the time series. The contributions from the three routines to the time series are: 50102–52028 MJD,

Table 3: Estimates of observational mean rates of topographic-height change, $\bar{u}_{\text{obs}}$, and gravity change, $\bar{\bar{g}}_{\text{obs}}$, their standard error, ϵ, and standard deviation, σ, based on GPS and absolute-gravimetry data for Churchill. The original data were provided by GSC (Lambert et al., 1994, 1996, 1998, 2001), GSD (Larson & van Dam, 2000; Lambert et al., 2001), IGS (Larson & van Dam, 2000; Park et al., 2002; this study), NGS (Lambert et al., 1994) and NOAA (Lambert et al., 1996, 1998, 2001; Larson & van Dam, 2000). The rates of Larson & van Dam (2000) are estimated from their Figure 4.

Author(s)	Obs. interval	$\bar{u}_{\text{obs}}$ (mm/a)	$\bar{\bar{g}}_{\text{obs}}$ (μGal/a)	ϵ (mm/a) (μGal/a)	σ (mm) (μGal)
Lambert et al. (1994)	1987–1991	–	−1.60	–	2.0
Lambert et al. (1996)	1987–1995	–	−1.45	0.19	1.6
Lambert et al. (1998)	1987–1995	–	−1.63	0.17	–
Larson & van Dam (2000)	1993–1999	–	−1.54	0.48	–
Larson & van Dam (2000)	1996–2000	10.7	–	0.23	–
Lambert et al. (2001)	1987–1999	–	−2.13	0.23	–
Park et al. (2002)	1995–1999	13.0	–	0.33	–
This study	1996–2003	11.4	–	0.70	–

52028–52510 MJD and 52510–52964 MJD for routines 3, 2 and 1, respectively. To reduce the computing time for data processing, the 273 GPS stations are grouped into four clusters. Each cluster itself constitutes a global network consisting of 80–100 stations. About 30 stations are common to all clusters and are used for combining the cluster solutions to the whole-network solution.

To determine the site velocities, two methods may be used (Dong et al., 2002). In the first method, the normal equations from all solutions for several years are combined and the site velocities for the stations are jointly estimated. The advantage of this method is that the full covariance matrix is used, *i.e.* all correlations are taken into account. Besides the high computational demands, its main disadvantage is that any position outliers or misfits for particular sites affect the estimates for all other sites. In the second method, position time series are constructed for each site separately from daily or weekly solutions and the site velocity is obtained by linear regression. The advantage of this method is that it is easier to control position outliers. Moreover, any misfit for one site does not affect the estimates for the other sites. Obviously, its weakness is that the correlation between individual time series is neglected. Since Zhang (1996) has shown these correlations to be small, we adopt the second method by constructing daily solutions.

To transform the time series into a unified reference frame, we refer the loosely constrained daily solutions to ITRF2000 (Altamimi et al., 2002) by a
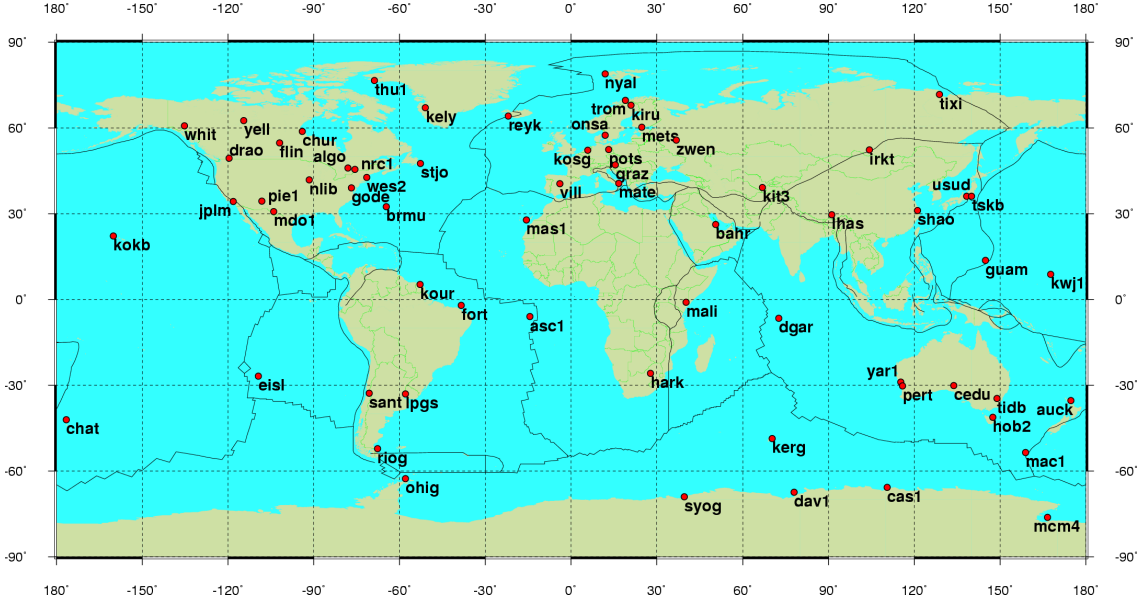
Figure 6: Locations of core GPS stations used for estimating parameters of Helmert transformation.

seven-parameter Helmert transformation:

$$
\begin{bmatrix} X \\ Y \\ Z \end{bmatrix}_{\text{ITRF}} = (1+c)\left(\begin{bmatrix} t_X \\ t_Y \\ t_Z \end{bmatrix} + \begin{bmatrix} 1 & r_Z & -r_Y \\ -r_Z & 1 & r_X \\ r_Y & -r_X & 1 \end{bmatrix} \begin{bmatrix} X \\ Y \\ Z \end{bmatrix}_{\text{LCRF}} \right), \quad (6)
$$

where (X, Y, Z) are the daily position coordinates, (t_X, t_Y, t_Z) the translation components, (r_X, r_Y, r_Z) the rotation angles, c is a dimensionless scaling term and the subscripts ITRF and LCRF indicate Cartesian coordinates in ITRF2000 and the loosely constrained reference frame, respectively. In total, 65 globally distributed high-quality core stations (Figure 6) are used for estimating the seven parameters of the Helmert transformation. Before it is implemented, the station coordinates given in ITRF2000 must be mapped to the epoch of the daily solution.

Next, mean position coordinates, $(\overline{X}, \overline{Y}, \overline{Z})$, are subtracted from the daily position coordinates $(X, Y, Z)_{\text{ITRF}}$, which gives the time series of residual position coordinates, $(\Delta X, \Delta Y, \Delta Z)$, in a body-fixed reference system. From this, time series for east, north and height coordinates, $(\Delta E, \Delta N, \Delta H)$, are obtained by transforming the residual coordinates from the body-fixed to a
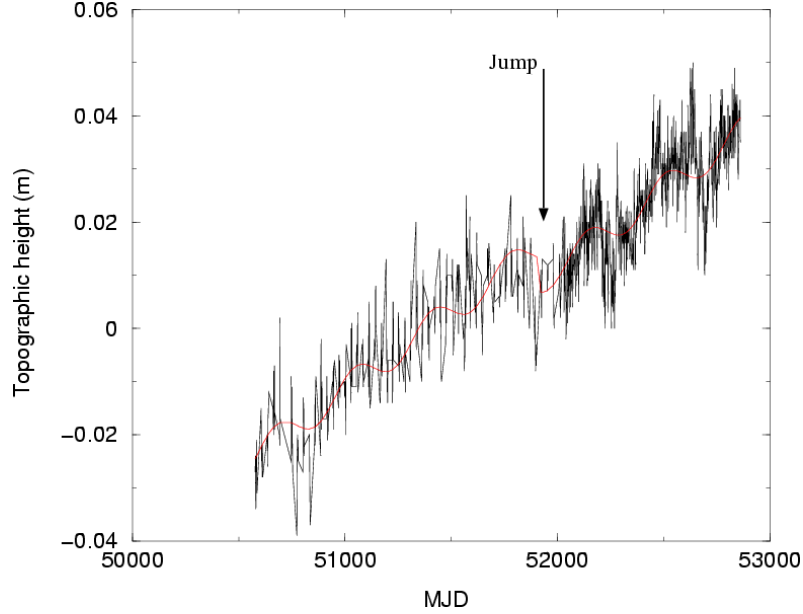
Figure 7: Height at Churchill according to GPS data. The annual wave (red curve) and the jump (arrow) are indicated.

topocentric coordinate system:

$$
\begin{bmatrix} \Delta E \\ \Delta N \\ \Delta H \end{bmatrix} = \begin{bmatrix} -\sin\lambda & \cos\lambda & 0 \\ -\cos\lambda\sin\varphi & -\sin\lambda\sin\varphi & \cos\varphi \\ \cos\lambda\cos\varphi & \sin\lambda\cos\varphi & \sin\varphi \end{bmatrix} \begin{bmatrix} \Delta X \\ \Delta Y \\ \Delta Z \end{bmatrix}, \qquad (7)
$$

where λ and φ are the station longitude and station latitude, respectively, and the vertical direction is defined as the radial direction with respect to the geocentre. The correlation information for (X, Y, Z) is used to propagate the error in $(\Delta X, \Delta Y, \Delta Z)$ to that in $(\Delta E, \Delta N, \Delta H)$.

Before estimating the linear trend for CHUR, its topographic-height time series is further analysed. This, in particular, requires the consideration of topographic-height changes caused by ocean loading, where the ocean-tide model FES95.2 is used. Also, semi-annual and annual sinusoidal waves must be removed, which have been found to contribute significantly to the variations of the station coordinates (*e.g.* van Dam et al., 2001; Crétaux & Soudarin, 2002; Dong et al., 2002; Zhang & Dong, 2002) and, thus, to influence the estimation of the linear trends (Blewitt & Lavallée, 2002). The offset observed for CHUR at 51902 MJD (December 24, 2000) is taken into account by a Heaviside step function with a jump of (-5.3 ± 0.22) mm (Figure 7). Finally, a weighted least-squares method is used for determining the observational mean rate of topographic-height change, $\bar{u}_{\mathrm{obs}}$ and its standard error, ϵ, with the values of

the time-series weighted according to their formal errors. Apart from the weighting, the procedure follows that outlined for the RSL height. The new rate is (11.4 ± 0.7) mm/a, which is close to the value of 10.7 mm/a obtained by Larson & van Dam (2000), but does not confirm that of 13.0 mm/a given by Park et al. (2002) (Table 3). However, the last value is probably less reliable, because no allowance was made for sinusoidal contributions.

The accuracy of the mean rate of topographic-height change estimated for CHUR may be improved by taking variations due to atmospheric loading into account. The problem goes back to Rabbel & Zschau (1985), who suggested atmospheric-pressure reductions to measurements of topographic height and gravity. Van Dam & Wahr (1987) and Van Dam et al. (1994) further studied the problem and found that peak-to-peak topographic-height changes caused by atmospheric-pressure variations may reach 15–20 mm. Besides semi-annual and annual variations automatically taken into account by fitting sinusoidal waves, the main contributors are storm-induced topographic-height changes dominated by periods of about two weeks. The application of appropriate corrections reduced the standard variation of the estimates for ∼60% of the investigated GPS stations (Van Dam et al., 1994; Brondeel & Willems, 2003). However, the results achieved are not completely satisfactory yet, the main reasons probably being inadequate atmospheric-pressure data or unrealistic earth models. For this reason, no atmospheric-loading reduction has been applied to the GPS data for CHUR so far.

5 SLI evidence of late- and post-glacial RSL height

In Canada, many marine features and associated organic materials had long been recognised as indicators of RSL-height changes. Since the first application of ^{14}C dating to the organic materials during the 1950s, it has become generally accepted that their age is late- or post-glacial. However, most samples provide only bounds for estimates of past sea levels. Thus, a marine shell indicates that the contemporaneous sea level lay above its topographic height, whereas a terrestrially deposited peat indicates that the sea level lay below its topographic height. In the following, any indicator of late- or post-glacial RSL height will be referred to as SLI.

5.1 Hudson Bay region

Early compilations of dated SLIs for Canada, including also the north-eastern USA, were provided by Farrand (1962), Walcott (1972) and others. On the supposition that the RSL height varies gradually with location, the SLIs were grouped into regions (Figure 8) and RSL diagrams constructed for each region (see Figure 9 for Churchill).

Attempts to estimate relaxation times for the RSL-height change observed in the Hudson Bay region go back to Andrews (1970), who fitted an exponential curve to the RSL heights and estimated a relaxation time of 1.76 ka. Later, Walcott (1980) constructed an RSL diagram for region HM[1] in southern Hudson Bay and calculated a relaxation time of at least 5 ka. This differs from the results of Mitrovica & Peltier (1993), who estimated much shorter relaxation times of 2.5, 3.3 and 2.0 ka for regions OI, SI and UP in northern Hudson Bay. Mitrovica & Peltier (1995) considered a larger assembly of regions in Hudson Bay. Whereas they retained the relaxation times for regions OI and UP, their new estimates for regions HM and SI were 17.9 and 4.9 ka, respectively. In addition, they determined relaxation times for the following regions: CH: 5.6 ka, JB: 1.5 ka, KW: 28.6 ka, RG: 7.6 ka, SI: 4.9 ka and UP: 2.0 ka. Mitrovica & Peltier ignored the times for regions CH and KW, because the SLIs they regarded as reliable span only time intervals of 3.0 and 1.2 ka, respectively. For the remaining regions, the agreement was found to be better in the north than in the south.

In view of the heterogeneity of the relaxation-time estimates, Peltier (1998) decided to construct a composite RSL diagram for south-eastern Hudson Bay based on SLIs collected over a broad region covering 51.5°–56.5°N and 76.5°–79.0°W. The relaxation time obtained according to the best-fitting exponential function is 3.426 ka.

In a fresh attempt, Mitrovica et al. (2000) argued that Peltier's (1998)

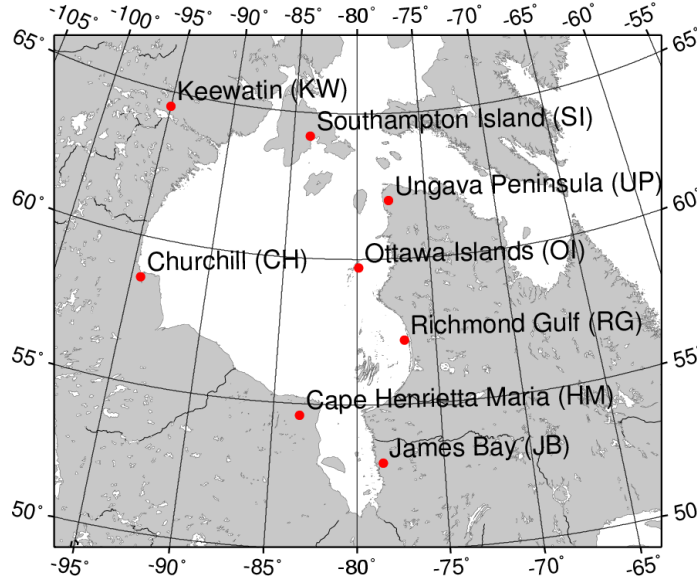[1]For abbreviations of the region names see Figure 8.

Figure 8: Map of SLI regions considered. Red circles denote the mean locations for the groups of SLIs. The abbreviations of the region names are given in brackets.

result is questionable, because it uses SLIs distributed over an area stretching roughly 600 km. At the same time, they pointed out a number of errors in previous estimates of relaxation times. Based on revised compilations of SLIs and taking into account eustatic sea-level changes, they inferred values of 2.0–2.8 ka and 4.0–6.6 ka for regions JB and RG, respectively.

5.2   Churchill region

The present study uses the SLI data base compiled for Canada by A. Dyke (pers. comm.) and is limited to 25 SLIs for region CH (Table 4). In the following, an SLI will represent a sample indicative of post-glacial sea level, for which latitude, φ, longitude, λ, RSL height (with respect to present-day sea level), s_{obs}, ^{14}C age, t_{C14}, and its standard error, ϵ_{C14}, have been determined. Depending on the type of sample, in our case shell (20), peat (2), bone (1), charcoal (1) or wood (1), and the type of deposition environment, an individual sample may represent an upper bound, a lower bound or a finite range for the RSL height at the time of deposition. The ^{14}C ages are reservoir corrected and based on a half-life of 5570 a. The calibrated ages correspond to the 'true' time of deposition before AD 1950. They are determined from t_{C14} and ϵ_{C14} using the 2σ-calibration mode of the program program `calib 4.1` (Stuiver & Reimer, 1993) providing upper and lower bounds, $t_{\mathrm{cal}}^{\mathrm{max}}$ and $t_{\mathrm{cal}}^{\mathrm{min}}$, respectively. The calibrated ages themselves and their standard errors then follow from

$t_{cal} = (t_{cal}^{min} + t_{cal}^{max})/2$ and $\epsilon_{cal} = (t_{cal}^{max} - t_{cal}^{min})/2$, respectively.

Conventionally SLIs from a particular region are combined in an RSL diagram displaying the time dependence of their RSL heights (Figure 9). In contrast to previous studies (*e.g.* Tushingham, 1992), where the RSL diagram refers to some average position, we retain the actual positions of the SLIs considered, because they are distributed over a region of $\sim(200 \times 200)$ km^2 (Figure 10).

Table 4: Characteristics of SLIs for region CH. For each sample are given ID No. according to internal data bank, longitude, λ, latitude, φ, RSL-height range, $s_{\mathrm{obs}}^{\mathrm{min}}$, $s_{\mathrm{obs}}^{\mathrm{max}}$, laboratory dating number, Lab. No., reservoir-corrected ^{14}C age, t_{C14}, its standard error, ϵ_{C14}, type of material and 2σ-calibrated age range, $t_{\mathrm{cal}}^{\mathrm{min}}$, $t_{\mathrm{cal}}^{\mathrm{max}}$. If $s_{\mathrm{obs}}^{\mathrm{min}}$ or $s_{\mathrm{obs}}^{\mathrm{max}}$ is not given, the sample represents an upper or lower bound on RSL height, respectively. If both $s_{\mathrm{obs}}^{\mathrm{min}}$ and $s_{\mathrm{obs}}^{\mathrm{max}}$ are given, the sample represents a finite range for RSL height. Ages are measured with respect to present time (AD 1950).

| ID No.	λ	φ	$s_{\mathrm{obs}}^{\mathrm{min}}$	$s_{\mathrm{obs}}^{\mathrm{max}}$	Lab. No.	t_{C14}	ϵ_{C14}	Material	$t_{\mathrm{cal}}^{\mathrm{min}}$	$t_{\mathrm{cal}}^{\mathrm{max}}$
	(°W)	(°N)	(m)	(m)		(a)	(a)		(a)	(a)
5162	94.7	58.1	67	145	Gx-1063	8010	95	shell	8600	9120
5152	95.417	57.667	–	134	GSC-3348	7760	370	shell	7955	9430
5151	95.833	58.55	106	165	GSC-3070	7770	140	shell	8325	9000
5161	95.05	58.183	142	–	GSC-92	7270	120	shell	7905	8305
5149	95.383	59.3	85	–	GSC-2579	6790	100	shell	7460	7815
5144	95.417	57.667	–	134	BGS-980	5960	100	peat	6530	7035
5143	94.237	58.39	0.3	–	BGS-796	5150	110	shell	5680	6155
5146	94.077	58.74	22	–	GSC-1549	5020	140	shell	5455	6065
5148	96.75	59.083	–	210	GSC-2567	4850	60	peat	5405	5730
5153	94.967	58.892	30	–	GSC-3851	4000	90	shell	4240	4740
5168	94.25	58.75	35	–	S-738	3560	105	shell	3590	4125
5142	95.0	57.967	–	100	BGS-793	3530	100	wood	3585	4050
5160	94.17	58.671	4	–	GSC-735	3430	140	shell	3405	4005
5163	94.275	59.75	38	–	Gx-1065	3190	80	shell	3260	3590
5164	93.657	58.607	30	–	Gx-1072	3190	80	shell	3260	3590
5158	93.811	58.619	38.5	–	GSC-685	3180	140	shell	3060	3690
5150	94.081	58.747	23	–	GSC-261	3040	130	shell	2895	3495
5167	94.25	58.75	–	30	S-521	2895	100	bone	2830	3260
5154	94.143	59.757	7	–	GSC-4507	2380	100	shell	2225	2695
5156	93.843	58.703	27	–	GSC-683	2320	130	shell	2095	2690
5159	93.981	58.757	22	–	GSC-723	2120	130	shell	1830	2360
5166	94.25	58.75	–	18	I-3973	2080	95	charcoal	1880	2260
5155	93.841	58.746	10.5	–	GSC-682	1240	130	shell	930	1355
5157	93.95	58.760	6.5	–	GSC-684	1020	140	shell	705	1180
5165	93.35	58.75	4	–	Gx-1073	385	80	shell	315	535
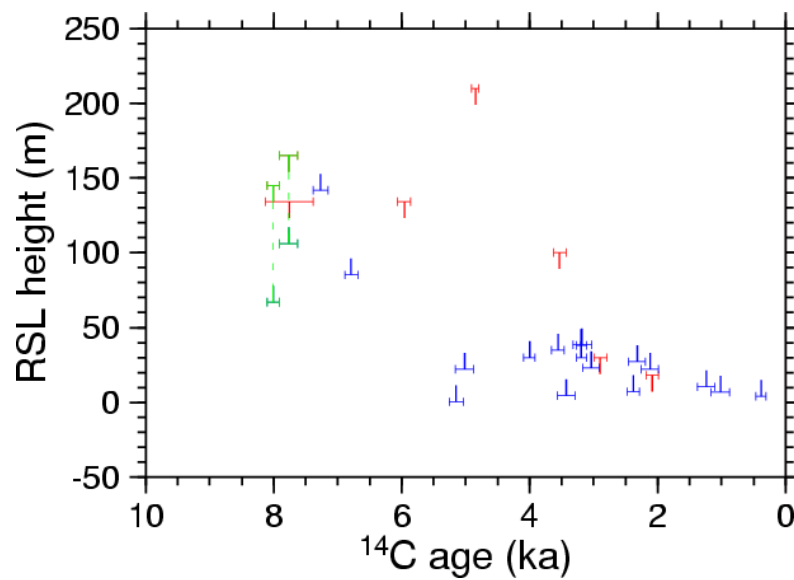
Figure 9: RSL diagram for region CH. SLIs are classified according to whether they provide upper bounds (red), lower bounds (blue) or finite ranges (green) for RSL height. Horizontal bars indicate standard errors of ^{14}C age.
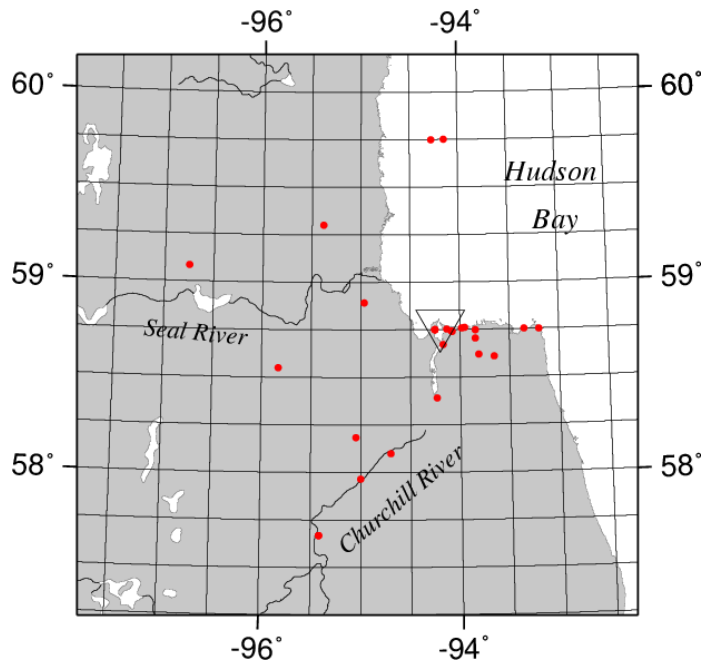

Figure 10: Map of region CH showing locations of SLIs (red dots) as well as tide-gauge and GPS stations (triangle).

6 Estimates of mantle viscosity

Whereas qualitative models of the process of GIA date back to the 19th century (see Wolf, 1993, for a historical review), quantitative models allowing estimates of the mantle viscosity have largely been developed after 1970 (see Peltier, 1998, 2004; Sabadini & Vermeersen, 2004, for recent reviews). At the beginning, most viscosity estimates were fully based on the late- and post-glacial RSL history documented by an increasingly dense global distribution of SLIs. More recently, the present-day adjustment recorded by ground-based or satellite-based geodetic techniques has been included as an additional constraint on the viscosity distribution.

In the following compilation, only those previous estimates of mantle viscosity that are either exclusively or predominantly based on the SLI evidence from the Hudson Bay region will be considered.

6.1 Previous estimates

Irrespective of the inconsistencies associated with the SLIs from the Hudson Bay region (Figure 8), attempts to infer the mantle viscosity from the data are numerous. One of the first interpretations is due to Nakada (1983), who considered regions CH, HM, OI and SI. Fixing the upper-mantle thickness below the lithosphere to 200 km and the lower-mantle viscosity to 10^{23} Pa s, he found that the upper-mantle viscosity required for the Hudson Bay region ranges between 0.05 and 0.75×10^{21} Pa s. If region CH is considered separately, the upper-mantle viscosity inferred is $\sim 0.5 \times 10^{21}$ Pa s. As Nakada pointed out, these models also satisfy the free-air gravity anomaly observed over Hudson Bay, which is, however, more recently believed to be partially related to mantle convection (Mitrovica, 1997; Simons & Hager, 1997).

Peltier & Andrews (1983) considered RSL data from regions CH, RG and OI supplemented by data from the North American east coast (EC) and and the free-air gravity anomaly over Hudson Bay. They found that upper- and lower-mantle viscosities of 10^{21} Pa s and $1–3 \times 10^{21}$ Pa s, respectively, fit the data most closely. In order to explain the free-air gravity anomaly with reduced viscosity values in the lower mantle, they invoked internal modes of relaxation associated with the density stratification of the earth model used in their interpretation.

Nakada & Lambeck (1991) investigated whether indications exist that upper-mantle viscosities may vary globally and presented preliminary results for four regions in terms of an earth model with a two-layer mantle separated by a discontinuity at 670 km depth. Considering RSL data from regions CH, HM and OI, they found that optimum fits are obtained for $\eta_{\mathrm{UM}} = 0.4–0.6 \times 10^{21}$ Pa s and $\eta_{\mathrm{LM}} = 20–50 \times 10^{21}$ Pa s.

Mitrovica & Peltier (1992) studied the depth resolution of the RSL data from the Hudson Bay region. Disregarding the free-air gravity anomaly, they

showed that the RSL history for regions JB, KW, OI, RG, SI and UP can be explained by a model with an upper-mantle viscosity of 10^{21} Pa s and a lower-mantle viscosity of 1–3×10^{21} Pa s, thus confirming the result of Peltier & Andrews (1983). Investigating the sensitivity kernels, they also showed that the data are most sensitive to viscosity variations in the very deepest regions of the upper mantle and in the top half of the lower mantle. With a two-layer lower mantle, the lower-mantle viscosity above 1800 km depth was found to be near 10^{21} Pa s, but a significant increase at larger depths cannot be ruled out.

Mitrovica & Peltier (1993) continued their study of the resolving power of the Hudson Bay RSL data on the basis of their estimates of the relaxation times for regions OI, SI and UP. Using a time window extending 6 ka backwards from today, their inversion confirmed the limited resolution in the bottom half of the lower mantle. The mean viscosity inferred for the depth range between 500 and 1870 km is 0.66–1.2×10^{21} Pa s.

Han & Wahr (1995) returned to the conventional viscosity parameterization in terms of two uniform layers separated by the 670-km discontinuity and considered RSL data from regions CH, HM, KW, OI, SI and UP supplemented by the free-air gravity anomaly over Hudson Bay. Using a single-disk model of the Laurentide ice sheet, they concluded that it is not possible to fit the RSL data from the six sites simultaneously. Best results were obtained for an upper-mantle viscosity of 0.6×10^{21} Pa s and a lower-mantle viscosity of 30×10^{21} Pa s. With an ice-sheet model consisting of four subdomes, a slightly improved fit of the data was achieved for an upper-mantle viscosity of 1.0×10^{21} Pa s and a lower-mantle viscosity of 50×10^{21} Pa s. If the free-air gravity anomaly was ignored, Han & Wahr could not rule out the value of 10^{21} Pa s for the lower-mantle viscosity.

Mitrovica & Peltier (1995) interpreted RSL data from regions HM, JB, OI, RG, SI and UP. Based on forward calculations, they found that, for two mantle layers separated by the 670-km discontinuity, the lower-mantle viscosity is in the range of 0.5–3×10^{21} Pa s. The upper-mantle viscosity was poorly resolved, but probably near 0.5×10^{21} Pa s. However, similar to other investigators, Mitrovica & Peltier concluded that no single earth model can reconcile the RSL record from all regions. Since the record for region HM appeared to be problematic due to a large time gap, it was excluded from the inverse modelling. The solution to the inverse problem for the depth range of maximum sensitivity to viscosity variations between 500 and 180 km resulted in viscosities between 0.71 and 1.1×10^{21} Pa s.

Forte & Mitrovica (1996) carried out joint inversions based on RSL diagrams for regions near the previous glaciation centres in Canada (Richmond Gulf, RG) and Sweden (Angerman River, AR) supplemented by long-wavelength geoid data. The viscosity profiles constructed show a significant jump by a factor of $\sim$10 near 1000-km depth. Between the surface and 1400-km depth, the viscosity was found to be 0.76×10^{21} Pa s. For the depth range

400–1800 km, a value of 1.9×10^{21} Pa s was obtained.

Mitrovica (1996) focused on RSL data from region RG, whose accuracy he regarded as comparable to that from region AR. Based on forward calculations, he showed that the RG relaxation time cannot be reconciled with a lower-mantle viscosity of less than 2.5×10^{21} Pa s. Based on a joint inversion of the RSL record from regions AR and RG, he furthermore showed that the weighted mean of the viscosity between 670-km and 2000-km depth is 1.4–3.3×10^{21} Pa s, where the viscosity increase between the upper mantle and the top 1000 km of the lower mantle is more than one order of magnitude. A joint inversion of relaxation times for regions AR, OI, SI and UP resulted in a weighted mean of the viscosity between 670-km and 2000-km depth of $\sim 0.79 \times 10^{21}$ Pa s.

Cianetti et al. (2002) interpreted the RSL data from regions CH, HM, JB, KW, OI, RG, SI and UP. Based on forward modelling, they found that the data can be reconciled by an upper-mantle viscosity of 10^{21} Pa s and a lower-mantle viscosity of 2×10^{21} Pa s. Using an inverse approach based on the Metropolis sampling algorithm, they further showed the RSL data from region CH suggest an essentially uniform mantle with upper- and lower-mantle viscosities of 3.2×10^{21} Pa s and 4.0×10^{21} Pa s, respectively. As found in previous studies, it was not possible to determine viscosity profiles that simultaneously matched RSL data from all regions within their uncertainties. The closest fit was reached for upper- and lower-mantle viscosities of 0.16×10^{21} Pa s and 2.0×10^{21} Pa s.

The results of the previous interpretations of the late- and post-glacial RSL record around Hudson Bay are compiled in Table 5.

6.2   New estimate based on joint inversion

In the following determination of mantle viscosity, we will use as observables for region CH the mean rate of RSL-height change, $\bar{\dot{s}}_{\mathrm{obs}} = (-9.72 \pm 0.26)$ mm/a (present study), the mean rate of topographic-height change, $\bar{\dot{u}}_{\mathrm{obs}} = (11.35 \pm 0.7)$ mm/a (present study), the mean rate of gravity change, $\bar{\dot{g}}_{\mathrm{obs}} = (-2.13 \pm 0.23)$ μGal/a (Lambert et al., 2001), and the late- and postglacial RSL height (Dyke, pers. comm.).

The last Pleistocene glaciation is simulated using the standard ice model ICE-3G (Tushingham & Peltier, 1991). The earth model employed is radially symmetric, self gravitating and viscoelastic, with the stratifications of the density and the elastic parameters according to PREM. To solve for the glaciation-induced perturbations of the field quantities, the spectral finite-element method (Martinec, 2000) is employed, where the earth-ice-ocean system is coupled by the sea-level equation (Wolf et al., 2002) accounting for the redistribution of melt water, geoid perturbations, moving coast lines and grounded ice. During the inversion procedure, the lithosphere thickness, h_{L}, is kept fixed at 100 km. The upper-mantle viscosity, η_{UM}, is varied between 0.1 and 3×10^{21} Pa s and the lower-mantle viscosity, η_{LM}, between 0.1 and
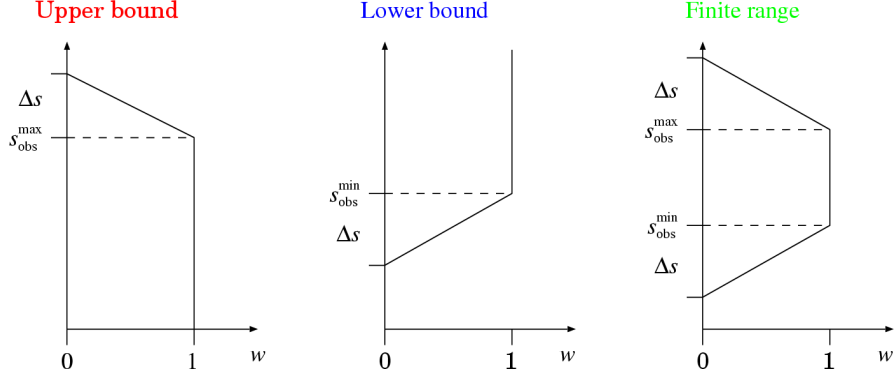
Figure 11: Membership functions, w, used for weighting of fits for RSL height.

3×10^{22} Pa s. Using these values, the rates of RSL-height change, topographic-height change and gravity change are calculated for the location of Churchill and the present time epoch, and the RSL height for the locations of the individual SLIs and the corresponding post-glacial time epochs. The program genesis used provides the radial, longitudinal and latitudinal displacement components, $(u_r, u_\lambda, u_\varphi)$, respectively, the local incremental gravitational potential, $\phi^{(\Delta)}$, and the local incremental gravity, $g^{(\Delta)}$. From these, the computational field quantities are defined:

$$\bar{\bar{u}}_{\text{com}} := \frac{u_r(t_2) - u_r(t_1)}{t_2 - t_1}, \tag{8}$$

$$\bar{\bar{s}}_{\text{com}} := -\frac{\phi^{(\Delta)}(t_2) - \phi^{(\Delta)}(t_1)}{g^{(0)}(t_2 - t_1)} - \bar{\bar{u}}_{\text{com}}, \tag{9}$$

$$\bar{\bar{g}}_{\text{com}} := -\frac{g^{(\Delta)}(t_2) - g^{(\Delta)}(t_1)}{t_2 - t_1} - \partial_r g^{(0)} \bar{\bar{u}}_{\text{com}}, \tag{10}$$

where $g^{(0)} = 9.81$ m/s^2 and $\partial_r g^{(0)} = -3.086 \times 10^{-6}$ s^{-2} are the unperturbed gravity and its gradient, respectively, and all quantities are evaluated at the earth's surface. The quality of the fit is evaluated using the magnitude of the difference between the computational and observational rates:

$$\chi(\bar{\bar{f}}) := |\bar{\bar{f}}_{\text{obs}} - \bar{\bar{f}}_{\text{com}}|, \tag{11}$$

where $\chi(\bar{\bar{f}})$ is the misfit function for $\bar{\bar{f}}$ representing $\bar{\bar{u}}$, $\bar{\bar{s}}$ or $\bar{\bar{g}}$.

For the interpretation of the late- and post-glacial height change, the computational RSL height, s_{com}, is compared with the corresponding observational RSL height, s_{obs}, with the weighting of the fit controlled by the constraints given by the SLIs according to a fuzzy scheme. More precisely, we assume that, for each SLI, the fit is quantified by a trapezoidal membership function, w, (Figure 11). For SLIs indicating an upper bound, $w = 1$ if the computational RSL height is below the bound, $s_{\text{com}} \leq s_{\text{obs}}^{\max}$. Conversely, for SLIs indicating

a lower bound, $w = 1$ if the computational RSL height is above the bound, $s_{\mathrm{com}} \geq s_{\mathrm{obs}}^{\mathrm{min}}$. For SLIs indicating a finite range, $w = 1$ if the computational RSL height is within the finite range, $s_{\mathrm{obs}}^{\mathrm{min}} \leq s_{\mathrm{com}} \leq s_{\mathrm{obs}}^{\mathrm{max}}$. The width of the linear ramps, Δs, where $0 < w < 1$, is determined according to $\Delta s = \dot{s}_{\mathrm{com}}\,\epsilon_{\mathrm{cal}}$, where $\dot{s}_{\mathrm{com}}$ is the computational rate of RSL-height change at the location and time epoch of deposition of the SLI. The misfit function for the RSL height, s, is then given by

$$\chi(s) := 1 - \frac{1}{P}\sum_{p=1}^{P} w_p(s_{\mathrm{obs}}, s_{\mathrm{com}}), \tag{12}$$

where P is the total number of SLIs considered and w_p is the membership function for the pth SLI.

Figure 12 shows the computational rates of RSL-height change, topographic-height change and gravity change as well as the differences to the corresponding observational rates as functions of upper- and lower-mantle viscosities. The contour patterns for the three types of observable are similar and the differences reach their minima (defined as one standard deviation of the observational rate) in nearly the same region of the parameter space. For the rates of RSL and gravity change, the best-fit regions are slightly smaller, with the observational rates absolutely larger than the best-fit computational rates. The optimum viscosity values are approximately $\eta_{\mathrm{UM}} = 3.2 \times 10^{20}$ Pa s and $\eta_{\mathrm{LM}} = 1.6 \times 10^{22}$ Pa s. For the rate of topographic-height change, the best-fit region is slightly larger and also more elongated. Figure 13 shows the fit achieved for the late- and post-glacial RSL height. The general pattern and best-fit region resemble those shown in Figure 12 and, thus, largely confirm the results obtained for the present-day rates.

To compare the results for the individual observables more closely, we superimpose the best-fit parameter regions successively (Figure 14). As indicated above, the rates of RSL and gravity change constrain the upper- and lower-mantle viscosities most closely. The best-fit regions for the rate of topographic-height change and for the late- and post-glacial RSL height are somewhat broader, but not in conflict with the results obtained for the other observables.

Table 5: Previous estimates of mantle viscosity, η_1, η_2, for specified depth ranges, d_1, d_2, respectively, based on SLIs from the Hudson Bay region according to Nakada (1983) (N83), Peltier & Andrews (1983) (PA83), Nakada & Lambeck (1991) (NL91), Mitrovica & Peltier (1992) (MP92), Mitrovica & Peltier (1993) (MP93), Han & Wahr (1995) (HW95), Mitrovica & Peltier (1995) (MP95), Forte & Mitrovica (1996) (FM96), Mitrovica (1996) (M96) and Cianetti et al. (2002) (CGS02). The SLIs considered have been grouped according to RSL diagrams for regions CH, HM, JB, KW, OI, RG, SI and UP (Figure 8) and the North American east coast (EC). The additional consideration of the free-air gravity anomaly over Hudson Bay is indicated by $*$, that of the long-wavelength non-hydrostatic geoid by $\dagger$ and that of SLIs from region AG (Sweden) by $\S$. Results based on formal inversions of the data are denoted by $\P$.

| Author(s)	d_1 (km)	η_1 (10^{21} Pa s)	d_2 (km)	η_2 (10^{21} Pa s)	SLI region(s)
N83	0–200	0.5	200–2900	100	CH, $*$
	0–200	0.05–0.75	200–2900	100	CH, HM, OI, SI, $*$
PA83	0–670	1	670–2900	1–3	CH, RG, OI, EC, $*$
NL91	0–670	0.4–0.6	670–2900	20–50	CH, HM, OI
MP92	0–670	1	670–2900	1–3	JB, KW, OI, RG, SI, UP
	670–1800	1	–	–	JB, KW, OI, RG, SI, UP, $\P$
MP93	500–1870	0.66–1.2	–	–	OI, SI, UP, $\P$
HW95	0–670	0.6–1	670–2900	30–50	CH, HM, KW, OI, SI, UP, $*$
MP95	0–670	0.5	670–2900	0.5–3	HM, JB, OI, RG, SI, UP
	500–1870	0.71–1.1	–	–	JB, OI, RG, SI, UP, $\P$
FM96	0–1400	0.76	–	–	RG, $\dagger$ $\S$ $\P$
	400–1800	1.9	–	–	RG, $\dagger$ $\S$ $\P$
M96	670–2900	> 2.4	–	–	RG
	670–2000	1.4–3.3	–	–	RG, $\S$ $\P$
	670–2000	0.79	–	–	OI, SI, UP, $\S$ $\P$
CGS02	0–670	1	670–2900	2	CH, HM, JB, KW, OI, RG, SI, UP
	0–670	3.2	670–2900	4.0	CH, $\P$
	0–670	0.16	670–2900	2.0	CH, HM, JB, KW, OI, RG, SI, UP, $\P$
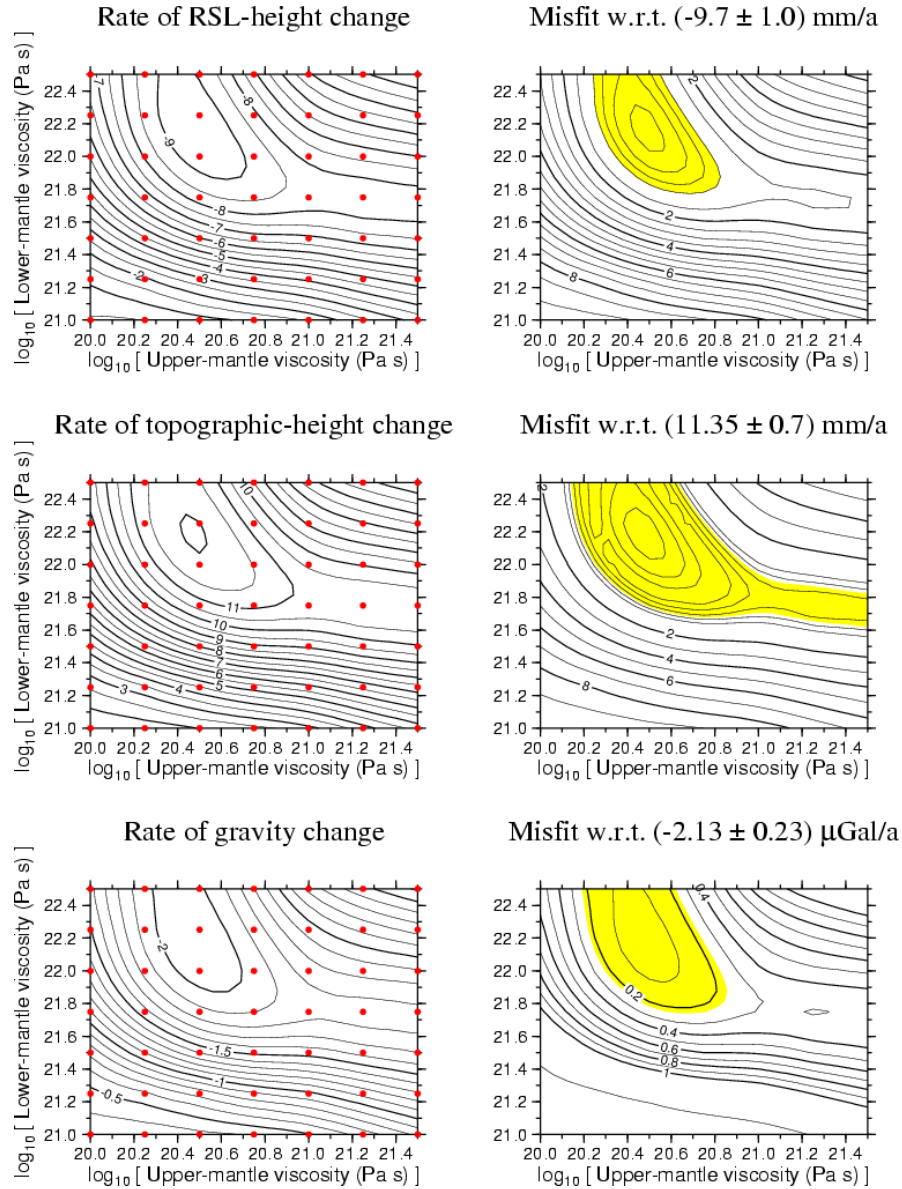
Figure 12: Computational rates of RSL-height change, height change and gravity change (left) as well as differences to corresponding observational rates (right) as functions of upper- and lower-mantle viscosities. In regions shown in yellow, the differences are smaller than the standard error of the appropriate observational rate.
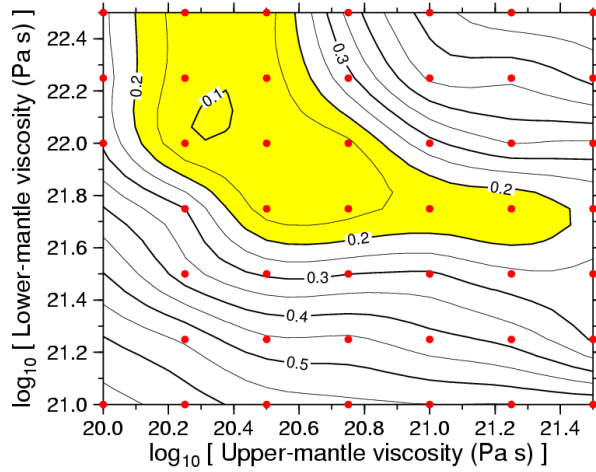
Figure 13: Misfit function for late- and post-glacial RSL height as function of upper- and lower-mantle viscosities. In regions shown in yellow, the misfit is smaller than 0.2.
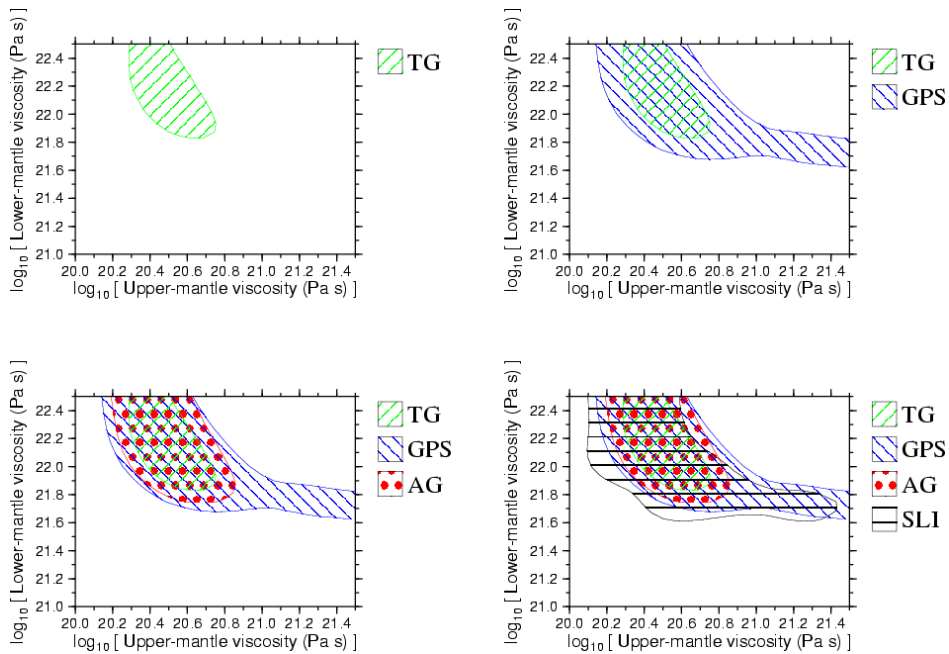

Figure 14: Best fits for rates of RSL-height change (TG), topographic-height change (GPS) and gravity change (AG) and for late- and post-glacial RSL height (SLI) as functions of upper- and lower-mantle viscosities. The individual regions correspond to the yellow regions in Figures 12 and 13.

7 Summary

The main results of our study are as follows:

We have extended the analysis of tide-gauge data for Churchill carried out by Tushingham (1992) using data from the last decade. As a new analysis tool, we have developed the linear-trend analysis diagram, which allows a systematic investigation of the linear trend in the RSL-height change as a function of the length of the observation interval and its mid-epoch. For short and intermediate observation intervals, the diagram displays considerable variability of the estimated linear trends, whence the IB-corrected mean rate of RSL-height change of (-9.72 ± 0.26) mm/a for the observation interval 1940–2001 is regarded as most reliable.

We have processed GPS data for Churchill using a time series from 1996–2001. Taking into account biannual and annual signals as well as allowing for a jump in the record, we have arrived at a mean rate of topographic-height change of (11.4 ± 0.7) mm/a.

We have considered 25 SLIs from the region CH, which are indicators of the RSL height during the past 9000 a. After analysing whether a sample provides an upper bound, a lower bound or a finite range for post-glacial RSL height, we have designed a fuzzy scheme in order to improve the results.

Finally, using ice model ICE-3G, a viscoelastic earth model with the upper- and lower-mantle viscosities as free parameters and the sea-level equation, we have inverted the present-day rates of RSL-height change, topographic-height change and gravity change as well as the late- and post-glacial RSL height in terms of mantle viscosity. All four types of observable return consistent best-fit parameter regions. The optimum values are $\sim 3 \times 10^{20}$ Pa s and $\sim 1.6 \times 10^{22}$ Pa s for the upper- and lower-mantle viscosities, respectively. Considering the uncertainties of the individual data sets, the constraint imposed on the lower-mantle viscosity can be relaxed such that values $>5 \times 10^{21}$ Pa s are indicated for it.

gram for the continuous wavelet transform was written by F. Barthelmes at GFZ. The Graphics program GMT (Wessel & Smith, 1991) was employed. This study was part of the SEAL project, BMBF Project No. SF2000/13.

References

Altamimi, Z., Sillard, P., & Boucher, C., 2002, ITRF2000: A new release of the International Terrestrial Reference Frame for earth science applications, *J. Geophys. Res.*, **107**, 2214, doi:10.1029/2001JB000561. 23

Andrews, J. T., 1970, Present and postglacial rates of uplift for glacial northern and eastern North America derived from postglacial uplift curves, *Can. J. Earth Sci.*, **7**, 703–715. 27

Barnett, D. M., 1966, A re-examination and re-interpretation of tide-gauge data for Churchill, Manitoba, *Can. J. Earth Sci.*, **3**, 77–88. 10, 11, 12, 20

Barnett, D. M., 1970, An amendment and extension of tide-gauge data analysis for Churchill, Manitoba, *Can. J. Earth Sci.*, **7**, 626–627. 10, 12, 20

Basnett, T. A. & Parker, D. E., 1997, *Development of the Global Mean Sea Level Pressure Data Set GSMLP2*, Clim. Res. Tech. Note, 79, Hadley Centre for Climate Prediction, Exeter. 15

Bell, R., 1896, Proofs of the rising of the land around Hudson Bay, *Am. J. Sci., Ser. 4*, **1**, 219–228. 6, 7, 8

Bird, J. B., 1954, Postglacial marine submergence in central Arctic Canada, *Bull. Geol. Soc. Am.*, **65**, 457–464. 8, 11

Bird, J. B., 1959, Recent contributions to the physiography of northern Canada, *Z. Geomorph.*, **3**, 151–174. 11

Blewitt, G. & Lavallée, D., 2002, Effect of annual signals on geodetic velocity, *J. Geophys. Res.*, **107**, 2145, doi:10.1029/2001JB000570. 25

Brondeel, M. & Willems, T., 2003, Atmospheric pressure loading in GPS height estimates, *Adv. Space Res.*, **31**, 1959–1964. 26

Cianetti, S., Giunchi, C., & Spada, G., 2002, Mantle viscosity beneath the Hudson Bay: an inversion based on the Metropolis algorithm, *J. Geophys. Res.*, **107**, 2352, doi:10.1029/2001JB000585. 34, 37

Cooke, H. C., 1942, Is the land around Hudson Bay at present rising?, *Am. J. Sci.*, **240**, 144–146. 8, 9

Crétaux, J.-F. & Soudarin, L., 2002, Seasonal and interannual geocenter motion from SLR and DORIS measurements: comparison with surface loading data, *J. Geophys. Res.*, **107**, 2374, doi:10.1029/2002JB001820. 25

Dohler, G. C. & Ku, L. F., 1970, Presentation and assessment of tides and water level records for geophysical investigations, *Can. J. Earth Sci.*, **7**, 607–625. 10, 12, 20

Dong, D., Fang, P., Bock, Y., Cheng, M. K., & Miyazaki, S., 2002, Anatomy

of apparent seasonal variations from GPS-derived site position time series, *J. Geophys. Res.*, **107**, 2075, doi:10.1029/2001JB000573.   23, 25

Douglas, B. C., 1991, Global sea level rise, *J. Geophys. Res.*, **96**, 6981–6992.   9

Douglas, B. C., 1997, Global sea rise: a redetermination, *Surv. Geophys.*, **18**, 279–292.   9

Douglas, B. C., Kearney, M. S., & Leatherman, S. P., eds., 2001, *Sea Level Rise: History and Consequences*, Academic Press, San Diego.   9

Ekman, M., 1996, A consistent map of the postglacial uplift of Fennoscandia, *Terra Nova*, **8**, 158–165.   9

Emery, K. O. & Aubrey, D. G., 1991, *Sea Levels, Land Levels, and Tide Gauges*, Springer, New York.   9

Fairbridge, R. W. & Hillaire-Marcel, C., 1977, An 8,000-yr palaeoclimatic record of the 'double-Hale' 45-yr solar cycle, *Nature*, **268**, 413–416.   8, 17

Farrand, W. R., 1962, Postglacial uplift in North America, *Am. J. Sci.*, **260**, 181–199.   27

Farrand, W. R. & Gajda, R. T., 1962, Isobases of the Wisconsin marine limit in Canada, *Geogr. Bull. Ottawa*, **17**, 5–22.   11

Forte, A. M. & Mitrovica, J. X., 1996, New inferences of mantle viscosity from joint inversion of long-wavelength mantle convection and post-glacial rebound data, *Geophys. Res. Lett.*, **23**, 1147–1150.   33, 37

Gendt, G., Dick, G., Mai, W., Nischan, T., & Sommerfeld, W., 1994, *Nutzerhandbuch zum Programmsystem EPOS.P.V2 (Earth Parameters and Orbit Determination System) für die Analyse von GPS-Daten*, Geo-ForschungsZentrum Potsdam, Potsdam.   22

Gough, W. A. & Robinson, C. A., 2000, Sea-level variation in Hudson Bay, Canada, from tide-gauge data, *Arct. Antarct. Alp. Res.*, **32**, 331–335.   13, 18

Gutenberg, B., 1941, Changes in sea level, postglacial uplift, and the mobility of the earth's interior, *Bull. Geol. Soc. Am.*, **52**, 721–772.   7, 9, 10, 11, 12

Gutenberg, B., 1942, Is the land around Hudson Bay at present rising?, *Am. J. Sci.*, **240**, 147–149.   8, 10, 12

Gutenberg, B., 1954, Postglacial uplift in the Great Lakes region, *Arch. Meteorol. Geophys. Bioklimatol., Ser. A*, **7**, 243–251.   10, 11, 12

Gutenberg, B., 1958, Rheological problems of the earth's interior, in *Rheology: Theory and Applications, Vol. 2*, edited by F. R. Eirich, pp. 401–431, Academic Press, New York.   11

Hagedoorn, J. M. & Wolf, D., 2003, Pleistocene and recent deglaciation in Svalbard: implications for tide-gauge, GPS and VLBI measurements, *J. Geodyn.*, **35**, 415–423.   5

Han, D. & Wahr, J., 1995, The viscoelastic relaxation of a realistically strat-

ified earth, and a further analysis of postglacial rebound, *Geophys. J. Int.*, **120**, 287–311. 33, 37

Hansell, R. I. C., Scott, P. A., Staniforth, R., & Svoboda, J., 1983, Permafrost development in the intertidal zone at Churchill, Manitoba: a possible mechanism for accelerated beach uplift, *Arctic*, **36**, 198–203. 12

Hillaire-Marcel, C. & Fairbridge, R. W., 1978, Isostasy and eustasy of Hudson Bay, *Geology*, **6**, 117–122. 8

Hubbard, B. B., 1997, *Wavelets, die Mathematik der kleinen Wellen*, Birkhäuser Verlag, Basel. 17

Jeffreys, H., 1952, *The Earth: Its Origin, History and Physical Constitution*, 3rd edn., Cambridge University Press, Cambridge. 7

Jeffreys, H., 1976, *The Earth: Its Origin, History and Physical Constitution*, 6th edn., Cambridge University Press, Cambridge. 7

Johnston, W. G., 1939, Recent changes of level of the land relative to sea level, *Am. J. Sci.*, **237**, 94–98. 7, 11

Lambeck, K., 1980, *The Earth's Variable Rotation: Geophysical Causes and Consequences*, Cambridge University Press, Cambridge. 14

Lambeck, K., Smither, C., & Ekman, M., 1998, Tests of glacial rebound models for Fennoscandinavia based on instrumented sea- and lake-level records, *Geophys. J. Int.*, **135**, 375–387. 9

Lambert, A., Liard, J. O., Courtier, N., Goodacre, A. K., & McConnell, R. K., 1989, Canadian absolute gravity program: applications in geodesy and geodynamics, *EOS, Trans. Am. Geophys. Union*, **70**, 1447, 1459, 1460. 21

Lambert, A., Liard, J. O., Courtier, N., & Bower, D. R., 1994, Absolute gravimetry applied to postglacial rebound studies: progress in Laurentia, in *Gravimetry and Space Techniques Applied to Geodynamics and Ocean Dynamics*, edited by B. E. Schutz, A. Anderson, C. Froidevaux, & M. Parke, pp. 1–7, American Geophysical Union, Washington. 21, 23

Lambert, A., James, T. S., Liard, J. O., & Courtier, N., 1996, The role and capability of absolute gravity measurement in determining the temporal variations in the earth's gravity field, in *Global Gravity Field and its Temporal Variations*, edited by R. H. Rapp, A. A. Cazenave, & R. S. Nerem, pp. 20–29, Springer, Berlin. 21, 23

Lambert, A., James, T. S., & Thorleifson, L. H., 1998, Combining geomorphological and geodetic data to determine postglacial tilting in Manitoba, *J. Palaeolimnol.*, **19**, 365–376. 21, 23

Lambert, A., Courtier, N., Sagawa, G. S., Klopping, F., Winester, D., James, T. M., & Liard, J. O., 2001, New constraints on Laurentide postglacial rebound from absolute gravity measurements, *Geophys. Res. Lett.*, **28**, 2109–2112. 21, 22, 23, 34

Larson, K. M. & van Dam, T., 2000, Measuring postglacial rebound with GPS

and absolute gravity, *Geophys. Res. Lett.*, **27**, 3925–3928.   22, 23, 26

Lisitzin, E., 1974, *Sea-Level Changes*, Elsevier, Amsterdam.   9

Manning, T. H., 1951, Remarks on the tides and driftwood strand lines along the east coast of James Bay, *Arctic*, **4**, 122–130.   8

Martinec, Z., 2000, Spectral–finite element approach for three-dimensional viscoelastic relaxation in a spherical earth, *Geophys. J. Int.*, **142**, 117–141.   34

Meier, M. F. & Wahr, J. M., 2002, Sea level is rising: Do we know why?, *Proc. Nat. Acad. Sci. Wash.*, **99**, 6524–6526.   9

Mitrovica, J. X., 1996, Haskell [1935] revisited, *J. Geophys. Res.*, **94**, 555–569.   34, 37

Mitrovica, J. X., 1997, Going halves over the Hudson Bay, *Nature*, **390**, 444–446.   32

Mitrovica, J. X. & Peltier, W. R., 1992, Constraints on mantle viscosity from relative sea level variations in Hudson Bay, *Geophys. Res. Lett.*, **19**, 1185–1188.   32, 37

Mitrovica, J. X. & Peltier, W. R., 1993, A new formalism for inferring mantle viscosity based on estimates of post glacial decay times: application to RSL variations in N.E. Hudson Bay, *Geophys. Res. Lett.*, **20**, 2183–2186.   27, 33, 37

Mitrovica, J. X. & Peltier, W. R., 1995, Constraints on mantle viscosity based upon the inversion of post-glacial uplift data from the Hudson Bay region, *Geophys. J. Int.*, **122**, 353–377.   27, 33, 37

Mitrovica, J. X., Forte, A. M., & Simons, M., 2000, A reappraisal of postglacial decay times from Richmond Gulf and James Bay, Canada, *Geophys. J. Int.*, **142**, 783–800.   27

Moore, S., 1948, Crustal movement in the Great Lakes area, *Bull. Geol. Soc. Am.*, **59**, 697–710.   7, 11

Nakada, M., 1983, Rheological structure of the earth's mantle derived from glacial rebound in Laurentide, *J. Phys. Earth.*, **31**, 349–386.   32, 37

Nakada, M. & Lambeck, K., 1991, Late Pleistocene and Holocene sea-level change; evidence for lateral mantle viscosity structure?, in *Glacial Isostasy, Sea Level and Mantle Rheology*, edited by R. Sabadini, K. Lambeck, & E. Boschi, pp. 79–94, Kluwer, Dordrecht.   32, 37

Park, K.-D., Nerem, R. S., Davis, J. L., Schenewerk, M. S., Milne, G. A., & Mitrovica, J. X., 2002, Investigation of glacial isostatic adjustment in the northeast U.S. using GPS measurements, *Geophys. Res. Lett.*, **29**, doi:10.1029/2001GL013782.   22, 23, 26

Peltier, W. R., 1998, Postglacial variations in the level of the sea: implications for climate dynamics and solid-earth geophysics, *Rev. Geophys.*, **36**, 603–689.   27, 32

Peltier, W. R., 2004, Global glacial isostasy and the surface of the ice-age earth: the ICE5G (VM2) model and GRACE, *Ann. Rev. Earth Planet. Sci.*, **32**, 111–149. 32

Peltier, W. R. & Andrews, J. T., 1983, Glacial geology and glacial isostasy of the Hudson Bay region, in *Shorelines and Isostasy*, edited by D. E. Smith & A. G. Dawson, pp. 285–319, Academic Press, London. 32, 33, 37

Peltier, W. R. & Douglas, B. C., 2002, The puzzle of global sea-level rise, *Phys. Today*, **55**, 35–40. 9

Plag, H.-P., 1988, *A Regional Study of Norwegian Coastal Long-Period Sea-Level Variations and their Causes*, Berliner Geowiss. Abh., Reihe B, 14, Dietrich Reimer Verlag, Berlin. 9

Rabbel, W. & Zschau, J., 1985, Static deformations and gravity changes at the earth's surface due to atmospheric loading, *J. Geophys.*, **56**, 81–99. 26

Sabadini, R. & Vermeersen, B., 2004, *Global Dynamics of the Earth— Applications of Normal Mode Relaxation Theory to Solid-Earth Geophysics*, Kluwer, Dordrecht. 32

Scherneck, H.-G., Johansson, J. M., Elgered, G., Davis, J. L., Jonsson, B., Hedling, G., Koivula, H., Ollikainen, M., Poutanen, M., Vermeer, M., Mitrovica, J. X., & Milne, G. A., 2002, BIFROST: observing the three-dimensional deformation of Fennoscandia, in *Ice Sheets, Sea Level and the Dynamic Earth*, edited by J. Mitrovica & L. L. A. Vermeersen, pp. 69–93, American Geophysical Union, Washington. 21

Simons, M. & Hager, B. H., 1997, Localization of the gravity field and the signature of glacial rebound, *Nature*, **390**, 500–504. 32

Stanley, G. M., 1939, Raised beaches on the east coast of James and Hudson Bays (abstract), *Bull. Geol. Soc. Am.*, **50**, 1936–1937. 7

Torrence, C. & Compo, G. P., 1998, A practical guide to wavelet analysis, *Bull. Am. Met. Soc.*, **79**, 61–78. 17

Tushingham, A. M., 1992, Observations of postglacial uplift at Churchill, Manitoba, *Can. J. Earth Sci.*, **29**, 2418–2425. 5, 10, 12, 13, 14, 20, 22, 29, 40

Tushingham, A. M. & Peltier, W. R., 1991, Ice-3G: a new approach of the late Pleistocene deglaciation based upon geophysical predictions of post-glacial relative sea level change, *J. Geophys. Res.*, **96**, 4497–4523. 22, 34

Tyrrell, J. B., 1894, Notes on the Pleistocene of the North-West Territories of Canada, north-west and west of Hudson Bay, *Geol. Mag.*, **1**, 395–399. 7

Tyrrell, J. B., 1896, Is the land around Hudson Bay at present rising?, *Am. J. Sci., Ser. 4*, **2**, 200–205. 6, 7

Van Dam, T. M. & Wahr, J. M., 1987, Displacement of the earth's surface due to atmospheric loading: effects on gravity and baseline measurements, *J. Geophys. Res.*, **92**, 1281–1286. 26

Van Dam, T. M., Blewitt, G., & Heflin, M. B., 1994, Atmospheric pressure

loading effects on Global Positioning System coordinate determinations, *J. Geophys. Res.*, **99**, 23939–23950.   26

van Dam, T. M., Wahr, J., Milly, P. C. D., Sihmakin, A. B., Blewitt, G., Lavallée, D., & Larson, K. M., 2001, Crustal displacements due to continental water loading, *Geophys. Res. Lett.*, **28**, 651–654.   25

Vaníček, P. & Nagy, D., 1979, *Report on the Compilation of the Map of Recent Crustal Movements in Canada*, Tech. Rep. 66, Dep. Surv. Eng. Univ. New Brunswick, Fredericton.   9, 10, 12, 13, 20

Walcott, R. I., 1972, Late Quaternary vertical movements in eastern North America: quantitative evidence of glacio-isostatic rebound., *Rev. Geophys. Space Phys.*, **10**, 849–884.   12, 27

Walcott, R. I., 1980, Rheological models and observational data of glacio-isostatic rebound, in *Earth Rheology, Isostasy, and Eustasy*, edited by N.-A. Mörner, pp. 3–10, J. Wiley, Chichester.   27

Wessel, P. & Smith, W. H. F., 1991, Free software helps map and display data, *EOS, Trans. Am. Geophys. Union*, **72**, 441–446.   41

Wolf, D., 1993, The changing role of the lithosphere in models of glacial isostasy: a historical review, *Global Planet. Change*, **8**, 95–106.   32

Wolf, D., Hagedoorn, J., & Martinec, Z., 2002, A new time-domain method of implementing the sea-level equation in glacial-isostatic adjustment, *EOS, Trans. Am. Geophys. Union*, **83** (Fall Meet. Suppl.), G12A–1059.   34

Zhang, F. P. & Dong, D., 2002, Seasonal vertical crustal motions in China detected by GPS, *Chinese Sci. Bull.*, **47**, 1772–1779.   25

Zhang, J., 1996, *Continuous GPS Measurements of Crustal Deformation in Southern California*, Ph.D. thesis, Univ. Calif., San Diego.   23

Mathematical symbols

Latin symbols

Symbol	Name
Symbol	*Name*
a	intercept
c	scaling term
$g^{(0)}$	unperturbed gravity
$g^{(\Delta)}$	local incremental gravity
$\bar{\dot{g}}_{\mathrm{com}}$	computational mean rate of gravity change
$\bar{\dot{g}}_{\mathrm{obs}}$	observational mean rate of gravity change
h_{L}	lithosphere thickness
N	total number of monthly values considered
P	total number of SLIs considered
(r_X, r_Y, r_Z)	rotation angles
s	RSL height
s_{com}	computational RSL height
s_{obs}	observational RSL height
$s_{\mathrm{obs}}^{\max}$	upper bound on observational RSL height
$s_{\mathrm{obs}}^{\min}$	lower bound on observational RSL height
Δs	width of linear ramps of membership function
s_{LR}	RSL height based on linear regression
s_n	monthly RSL height for nth month
$\bar{\dot{s}}_{\mathrm{com}}$	computational mean rate of RSL change
$\bar{\dot{s}}_{\mathrm{obs}}$	observational mean rate of RSL change
t	time epoch
t_{cal}	calibrated age
$t_{\mathrm{cal}}^{\max}$	upper bound on calibrated age
$t_{\mathrm{cal}}^{\min}$	lower bound on calibrated age
t_{C14}	^{14}C age
t_n	reference time epoch for s_n
(t_X, t_Y, t_Z)	translation components
$(u_r, u_\lambda, u_\varphi)$	radial, longitudinal and latitudinal displacement components
$\bar{\dot{u}}_{\mathrm{com}}$	computational mean rate of height change
$\bar{\dot{u}}_{\mathrm{obs}}$	observational mean rate of height change
w	membership function
w_p	membership function for pth SLI
(X, Y, Z)	daily position coordinates
$(\overline{X}, \overline{Y}, \overline{Z})$	mean position coordinates
$(\Delta X, \Delta Y, \Delta Z)$	residual position coordinates
$(\Delta E, \Delta N, \Delta H)$	east, north and height coordinates

Greek symbols

Symbol	Name
ϵ	standard error of $\bar{\dot{g}}_{\mathrm{obs}}$, $\bar{\dot{s}}_{\mathrm{obs}}$ or $\bar{\dot{u}}_{\mathrm{obs}}$
ϵ_{cal}	standard error of calibrated age
ϵ_{C14}	standard error of ^{14}C age
η_{LM}	lower-mantle viscosity
η_{UM}	upper-mantle viscosity
λ	longitude of station or SLI
σ	standard deviation
$\phi^{(\Delta)}$	local incremental gravitational potential
φ	latitude of station or SLI
$\chi(\bar{\dot{f}})$	misfit function for $\bar{\dot{f}}$
$\chi(s)$	misfit function for RSL height

Abbreviations

Abbreviation	Name
AR	Angerman River
BADC	British Atmospheric Data Centre
BMBF	Bundesministerium für Bildung und Forschung (Germany)
CH	Churchill
CHS	Canadian Hydrographic Service
CHUR	GPS station Churchill
EC	east coast of North America
EPOS	Earth Parameters and Orbit Determination System
GFZ	GeoForschungsZentrum Potsdam (Germany)
GMSLP2.1f	Global Mean Sea-Level Pressure v.2.1f
GSC	Geological Survey of Canada
GSD	Geodetic Survey Division (Canada)
HM	Cape Henrietta Maria
IB	inverse barometer
IGS	International GPS Service
ITRF	International Terrestrial Reference Frame
JB	James Bay
KW	Keewatin
LCRF	loosely constrained reference frame
MEDS	Marine Environmental Data Service (Canada)
MJD	modified Julian day
MSB	Marine Science Branch (Canada)
NGS	National Geodetic Survey (USA)
NOAA	National Oceanic and Atmospheric Administration (USA)

OI	Ottawa Islands
PSMSL	Permanent Service for Mean Sea Level
RLR	revised local reference
RSL	relative sea level
SEAL	Sea Level: An Integrated Approach to its Quantification
SI	Southampton Island
SLI	sea-level indicator
TIGA	GPS Tide Gauge Benchmark Monitoring – Pilot Project
UHSLC	University of Hawaii Sea Level Center (USA)
UP	Ungava Peninsula